THE JOURNAL OF PHYSICAL CHEMISTRY B
A JOURNAL OF THE AMERICAN CHEMICAL SOCIETY

pubs.acs.org/JPCB

Article

Understanding and Tailoring Excited State Properties in Solution-Processable Oligo(*p*-phenyleneethynylene)s: Highly Fluorescent Hybridized Local and Charge Transfer Character via Experiment and Theory

Hakan Usta,* Bunyemin Cosut,* and Fahri Alkan*

Cite This: *J. Phys. Chem. B* 2021, 125, 11717−11731

Read Online

ACCESS | Metrics & More | Article Recommendations | Supporting Information

ABSTRACT: Rod-shaped oligo(*p*-phenyleneethynylene) (OPE) offers an attractive π-framework for the development of solution-processable highly fluorescent molecules having tunable hybridized local and charge transfer (HLCT) excited states and (reverse) intersystem crossing ((R)ISC) channels. Herein, an HLCT oligo(*p*-phenyleneethynylene) library was studied for the first time in the literature in detail systematically via experiment and theory. The design, synthesis, and full characterization of a new highly fluorescent ($\Phi_{PL\text{-}solution} \sim 1$) sky blue emissive 4′,4‴-((2,5-bis((2-ethylhexyl)oxy)-1,4-phenylene)bis(ethyne-2,1-diyl))bis(*N*,*N*-diphenyl-[1,1′-biphenyl]-4-amine) (**2EHO-TPA-PE**) was also reported. The new molecule consists of a D′−Ar−π−D−π−Ar−D′ molecular architecture with an extended π-spacer and no acceptor unit, and detailed structural, physicochemical, single-crystal, and optoelectronic characterizations were performed. A high solid-state quantum efficiency ($\Phi_{PL\text{-}solid\ state} \sim 0.8$) was achieved as a result of suppressed exciton−phonon/vibronic couplings (no π−π interactions and multiple (14 per dimeric form) strong C−H···π interactions). Strong solution-phase/solid-state dipole-dependent tunable excited state behavior (local excited (LE) → HLCT → charge transfer (CT)) and decay dynamics covering a wide spectral region were demonstrated, and the CT state was observed to be highly fluorescent despite extremely large Stokes shift (∼130 nm)/fwhm (∼125 nm) and significant charge separation (0.75 charge·nm). Employing the Lippert−Mataga model, along with detailed photophysical studies and TDDFT calculations, key relationships between molecular design−electronic structure−exciton characteristics were elucidated with regards to HLCT and hot exciton channel formations. The interstate coupling between CT and LE states and the interplay of this coupling with respect to medium polarity were explored. A key relationship between excited-state symmetry breaking process and the formation of HLCT state was discussed for TPA-ended rod-shaped OPE π-systems. (R)ISC-related delayed fluorescence ($\tau \sim 2$−6 ns) processes were evident following the prompt decays (∼0.4−0.9 ns) both in the solution and in the solid-state. As a unique observation, the delayed fluorescence could be tuned and facilitated via small dielectric changes in the medium. Our results and the molecular engineering perspectives presented in this study may provide unique insights into the structural and electronic factors governing tunable excited state and hot-exciton channel formations in OPEs for (un)conventional solution-processed luminescence applications.

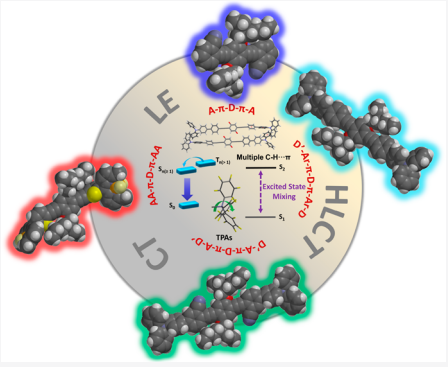

INTRODUCTION

Molecular systems embedding donor/acceptor−π−donor/acceptor (D/A−π−D/A) frameworks are a new exciting class of luminescent materials showing hybridized local and charge transfer (HLCT) excited states and high photo/electroluminescence efficiencies.[1−4] These molecules, when combined with solution processability[5,6] and synthetic versatility[7] enabling ease of fabrication and tunable color/functionality, offer great advantages in new generation lighting, display, and sensing applications.[2,8−16] When compared with traditional fluorescent materials, which could utilize only 25% of electrically generated excitons (radiative exciton yield (η_r)) for light emission as controlled by spin statistics and spin-allowed electronic transitions,[17] the HLCT characteristics of the singlet and triplet excited states could allow for additional population of excitons in the emissive S_1 excited state.[18−20] In fluorescent molecules with HLCT excited states, this is enabled by a reverse intersystem crossing (RISC) process from higher energy triplet excited state(s) (T_m ($m > 1$)) to the singlet excited state(s) (S_n ($n \geq 1$), which is also called hot-exciton channel and results in high η_r's of ≫25%.[21] This approach, following Ma and Yang et al.'s initial

Received: August 12, 2021
Revised: September 24, 2021
Published: October 13, 2021

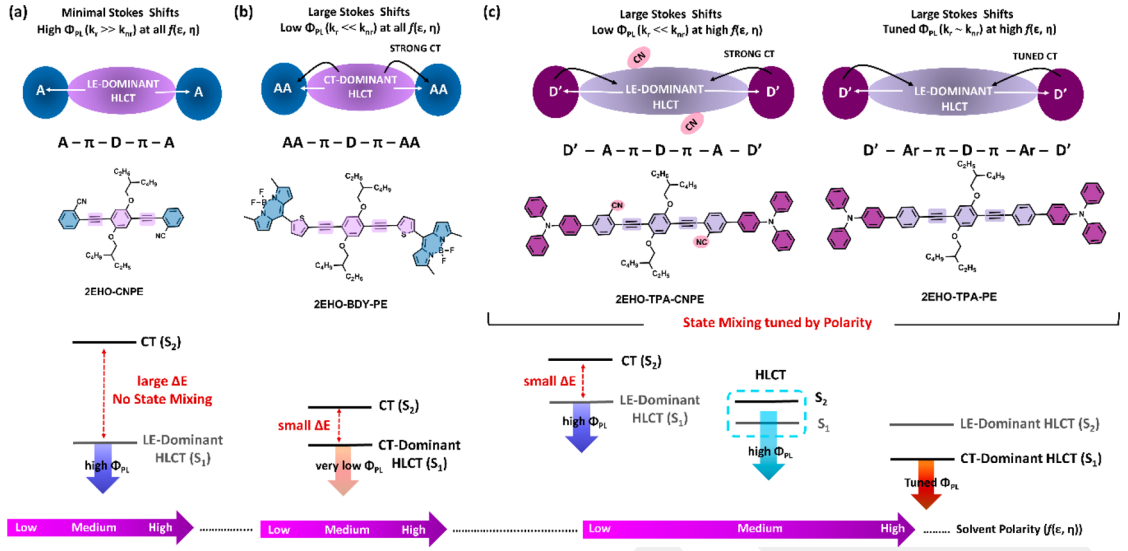

Figure 1. Molecular π-architectures and chemical structures of deep-blue emissive **2EHO-CNPE** (a), nonemissive **2EHO-BDY-PE** (b), and green emissive **2EHO-TPA-CNPE** (c, left) molecules developed in our earlier studies,[35−37] and the new sky blue emissive **2EHO-TPA-PE** (c, right) molecule developed in this study. The illustration of hybridized local and charge transfer (HLCT) and (weak/strong/tuned) charge transfer (CT) excited states formation on the OPE π-backbone and the corresponding electron transfers. S_1 and S_2 states mixing tuned by solvent polarity. AA denotes a stronger acceptor unit relative to A, and the bottom pink arrow indicates a solvent polarity increase.

report in 2012,[22] has become an attractive avenue to realizing highly fluorescent molecules and achieving high performance electroluminescent devices.[2] Although RISC channels in the upper excited states (T_m ($m > 1$) → S_n ($n \geq 1$)) is an exception to Kasha's rule in photochemistry,[23] upon meeting proper energetic conditions ($\Delta E_{S_n-T_m} \ll \Delta E_{T_m-T_{m-1}}$ for $k_{RISC} \gg k_{IC(T)}$) and effective hybridization of locally excited (LE) and charge-transfer (CT) characteristics in the corresponding excited states, this process could be very fast (lifetime ∼ several nanoseconds) and compete with the triplet state internal conversions.[9] The utilization of hot-exciton channels in HLCT molecules prevents the accumulation of relatively long-lived T_1 excitons, which could otherwise lead to undesired triplet−triplet annihilation or singlet−triplet quenching, as typically seen in thermally activated delayed-fluorescence (TADF).[24,25] In the design of HLCT fluorescent molecules, while the CT character with spatially separated hole/electron wave functions reduces the corresponding singlet−triplet excited state energy splitting (quasi-degenerate singlet and triplet excitons with $\Delta E_{ST} \sim 0$ eV) and facilitates R(ISC) processes,[26] the LE character with large orbital overlap between electron and hole wave functions induces a large transitional dipole moment (efficient $S_1 \rightarrow S_0$ fluorescence emission).[27]

Among varied π-conjugated molecular families studied in the past decade, rod-shaped oligo(*p*-phenyleneethynylene)-based molecules (OPEs) have been demonstrated to show tunable photoluminescence properties with high solution/solid-state quantum yields upon functionalization with donor (D) and/or acceptor (A) units.[28−31] Despite these reports, OPEs have not played a major role in electroluminescent devices, and the known few examples had shown limited performances (external quantum efficiencies (EQE_{max}s) < 2.5% in organic light-emitting diodes (OLEDs)).[32−34] In our recent works, however, we have engineered the OPE π-system into favorable A−π−D−π−A and D′−A−π−D−π−A−D′ architectures to yield solution-processable deep-blue emissive **2EHO-CNPE**[35] and green emissive **2EHO-TPA-CNPE**[36] molecules (Figure 1a and 1c). For the first time in the literature, we demonstrated HLCT excited state and hot-exciton channel formations for a thin film of an OPE molecule. As a result of its ideal electronic structure and optical properties, these OPE molecules demonstrated high radiative exciton yields (η_r = 60−70% ≫ 25% of singlet-state spin statistics) during electroluminescence, and **2EHO-CNPE** achieved one of the highest performances (EQE_{max} > 7% in OLEDs) reported to date for a solution-processed deep-blue OLED. On the other hand, in contrary to these highly fluorescent OPE π-frameworks, another OPE molecule developed in our research group, **2EHO-BDY-PE** (Figure 1b), showed extremely poor photoluminescence properties ($\Phi_{PL} \sim 0.02$) as a result of its strong charge-transfer excited state character.[37] Considering all the aforementioned luminescence properties and our recent findings, we believe that continuous efforts to develop new OPE π-architectures are very crucial to expand the library of OPE-based molecules and to elucidate HLCT design rationales with regards to excited state/electronic transition characteristics.

In this contribution, we demonstrate the molecular design, synthesis, and full characterization of a new sky blue emissive OPE molecule, 4′,4‴-((2,5-bis((2-ethylhexyl)oxy)-1,4-phenylene)bis(ethyne-2,1-diyl))bis(*N*,*N*-diphenyl-[1,1′-biphenyl]-4-amine) (**2EHO-TPA-PE**) (Figure 1c), in a D′−Ar−π−D−π−Ar−D′ molecular architecture. Different than our previous molecules, this new rod-shaped molecule does not include a strong acceptor unit and it employs an extended π-spacer (ethynylene−phenylene (π−Ar)). **2EHO-TPA-PE** showed high photoluminescence quantum efficiency ($\Phi_{PL\text{-solution}} \sim 1$) and strong solution-phase/solid-state medium dipole-dependent excited-state behavior covering the 400−650 nm spectral region. The absence of π−π interactions, along with the presence of multiple (14 interaction per dimeric form) strong C−H···π interactions, lead to a high solid-state quantum efficiency ($\Phi_{PL\text{-solid state}} \sim 0.80$). Significant changes in the excited state characteristics (LE-Dominant → HLCT → CT-Dominant), energies (λ_{PL}^{max} = +90 nm), and decay kinetics were observed upon polarity increase. The excitonic transformation was also evident in the solid-state for spin-coated **2EHO-TPA-**

https://doi.org/10.1021/acs.jpcb.1c07165
J. Phys. Chem. B 2021, 125, 11717−11731

PE-doped polymer and neat thin-films. The new molecule, as a result of its current π-spacer extended D′−Ar−π−D−π−Ar−D′ architecture without a strong acceptor unit, showed a tuned CT excited state character ($k_r \sim k_{nr}$) with highly red-shifted yet still intense ($\Phi_{PL} \sim 0.50$ and $\tau \sim 2.25$ ns) fluorescence properties. Different than low and high polarity solvent media, in medium-polarity solvents, delayed fluorescence decays (~2−6 ns with 3−11% contributions) were measured following the prompt decays (~0.4−0.9 ns). In this region, even a subtle polarity change was found to facilitate delayed fluorescence dynamics. This is attributed to high-lying (R)ISCs, and to the best of our knowledge, the polarity dependence of this process has not been reported previously. Finally, by combining our detailed photophysical findings with TDDFT calculations, we demonstrate for the first time a systematic study on a library of HLCT OPE molecules and reveal the molecular design−electronic structure−exciton characteristics relationships with regard to LE vs. HLCT vs. CT excited states and (R)ISC channel formations. A unique relationship between excited-state symmetry breaking process and the formation of the HLCT state is discussed for TPA-ended rod-shaped OPE π-systems.

MATERIALS AND METHODS

Materials, Methods, and Characterizations. All reagents were purchased from commercial sources and used as received without further purification. All reactions were carried out under N_2 atmosphere, and Schlenk techniques were employed. ^{1}H (400 MHz) and ^{13}C (100 MHz) NMR spectra were recorded using a Bruker 400 spectrometer. MALDI−TOF characterization was performed on a Bruker Microflex LT MALDI−TOF−MS instrument. Elemental analyses were performed using a LecoTruspec Micro model instrument. Thermal characterizations (i.e., thermogravimetric analysis (TGA) and differential scanning calorimetry (DSC)) were performed under nitrogen at a heating rate of 10 °C min^{-1} using Mettler Toledo-TGA/STDA 851 and Mettler Toledo-DSC 822 model instruments, respectively. UV−vis absorption spectra were recorded on a Shimadzu, UV-1800 UV−vis spectrophotometer. Photoluminescence (PL) characterizations were carried out with a Varian Eclipse spectrofluorometer. Time-correlated single photon counting measurements were performed on a Horriba-Jobin-Yvon-SPEX Fluorolog 3-2iHR instrument with 390 nm pulsed laser diode and Fluoro Hub-B single photon counting controller. The PL quantum yields in solid-state (single-crystal solid and spin-coated thin-film) and solution were measured on a Hamamatsu absolute PL quantum yield spectrometer, model C11347, using the integrating-sphere method and in dichloromethane as compared to the fluorescence of quinine sulfate standard (Φ_{PL} = 0.54 in 0.1 N H_2SO_4), respectively (λ_{exc} = 370 nm). Electrochemical measurements were carried out on a BAS-Epsilon potentiostat/galvanostat from Bioanalytical Systems Inc. (Lafayette, IN) equipped with a C3-cell stand. **2EHO-TPA-PE**-doped PS or PMMA thin-films (~40 nm) and the neat thin-film (~40 nm) were prepared by spin-coating (1200 rpm for 60 s, SCS G3 Spin Coater) **2EHO-TPA-PE** (0.15 mg) added PS or PMMA solutions (5 mg/mL) and **2EHO-TPA-PE** solution (5 mg/mL) in chloroform, respectively.

Theoretical Calculations and Methods. All calculations were performed with Gaussian 09[38] program package using B3LYP functional[39,40] and 6-311g** basis set. This level of theory has been employed by our group previously for OPE-π systems, and it showed good agreement with the experiment in terms of HOMO/LUMO energies, UV−vis spectra, and emission energies.[35,36] Geometry optimizations were followed by excited state calculations using TDDFT formalism as implemented in Gaussian. The Multiwfn[41] software was employed to calculate transition density matrices (TDMs) and Λ parameters[42] for the excited-state analysis of OPE-π systems.

Synthesis and Structural Characterization. Prior to the following final step, the synthesis of **2EHO-DEB** was carried out in accordance with our previously reported procedure,[36] and the intermediate compound **2EHO-Br-PE** was synthesized via halogen-selective Sonogashira cross-coupling reaction between **2EHO-DEB** and 1-bromo-4-iodobenzene in 65% yield (see the Supporting Information for details).

Synthesis of 4′,4‴-((2,5-Bis((2-ethylhexyl)oxy)-1,4-phenylene)bis(ethyne-2,1-diyl))bis(*N*,*N*-diphenyl-[1,1′-biphenyl]-4-amine) (2EHO-TPA-PE). The solution of 4,4′-((2,5-bis((2-ethylhexyl)oxy)-1,4-phenylene)bis(ethyne-2,1-diyl))bis(bromobenzene) (**2EHO-Br-PE**) (0.277 g, 0.400 mmol) and 4-(diphenylamino)phenylboronic acid pinacol ester (0.304 g, 0.82 mmol) in 15 mL of dimethoxyethane (DME) was stirred at room temperature for 5 min. Then, $Pd(PPh_3)_4$ (0.022 g, 0.019 mmol) and Na_2CO_3 (0.395 g, 3.73 mmol) in 5 mL of water were added, and the resulting mixture was heated at 80 °C under nitrogen for 24 h. After the reaction was completed, the mixture was cooled to room temperature and quenched with water. The reaction mixture was then extracted with chloroform, and the organic phase was washed with water, dried over Na_2SO_4, filtered, and evaporated to dryness to give a crude product. The crude product was then purified by column chromatography on silica gel using a dichloromethane:hexanes (3:1) solvent mixture to afford **2EHO-TPA-PE** as a pure yellow solid (0.237 g, 58% yield). ^{1}H NMR (400 MHz, $CDCl_3$): δ 7.59 (4H, broad s), 7.51 (2H, d, J = 8 Hz), 7.30 (4H, m), 7.15 (6 H, broad d, J = 8 Hz), 7.05 (3H, m), 3.96 (2H, m), 1.84 (1H, m), 1.28−1.67 (8H, m), 1.00 (3H, t, J = 12 Hz), 0.91 (3H, t, J = 12 Hz). ^{13}C NMR (100 MHz, $CDCl_3$): δ 153.9, 147.5, 140.3, 134.0, 131.9, 129.3, 127.6, 126.4, 124.4, 123.6, 123.0, 121.9, 116.5, 113.9, 112.9, 94.9, 86.7, 72.0, 39.7, 30.7, 29.3, 28.9, 24.0, 23.1, 14.1, 11.3. T_{mp} = 164−165 °C. MS (MALDI−TOF) m/z (M^+): calcd for $C_{74}H_{72}N_2O_2$, 1020.56; found, 1020.11for $[M]^+$. Anal. Calcd for $C_{74}H_{72}N_2O_2$: C, 87.02; H, 7.11; N, 2.74. Found: C, 87.35; H, 7.21; N, 2.88.

RESULTS AND DISCUSSION

Molecular Design, Synthesis, Structural Characterization, and Thermal Properties. The rod-shaped D′−Ar−π−D−π−Ar−D′ molecular architecture of **2EHO-TPA-PE** include triphenylamine (D′) and dialkoxyphenylene (D) donor units, and ethynylene (π) and unsubstituted phenylene (Ar) π-spacers. This design is different than our previously reported deep blue and green fluorescent molecules; it does not include an acceptor and π-spacing unit is extended. The rationale that the extended OPE π-system is retained but cyano units are removed is envisioned to give an efficient sky blue fluorescence with a color coordinate in between green and deep blue emission. This new molecule is also expected to guide us to understand whether D−π−D′ architecture in OPEs would be as useful for HLCT formation as D−π−A. The good solubility of the new molecule would be provided by highly twisted aryl substituents (*vide infra*) and swallow-tailed alkyl substituents. Ethynylene and phenylene units are placed between two donor units to control the electronic structure and the optical band gap and to facilitate efficient fluorescence emission by tuning HLCT

https://doi.org/10.1021/acs.jpcb.1c07165
J. Phys. Chem. B 2021, 125, 11717−11731

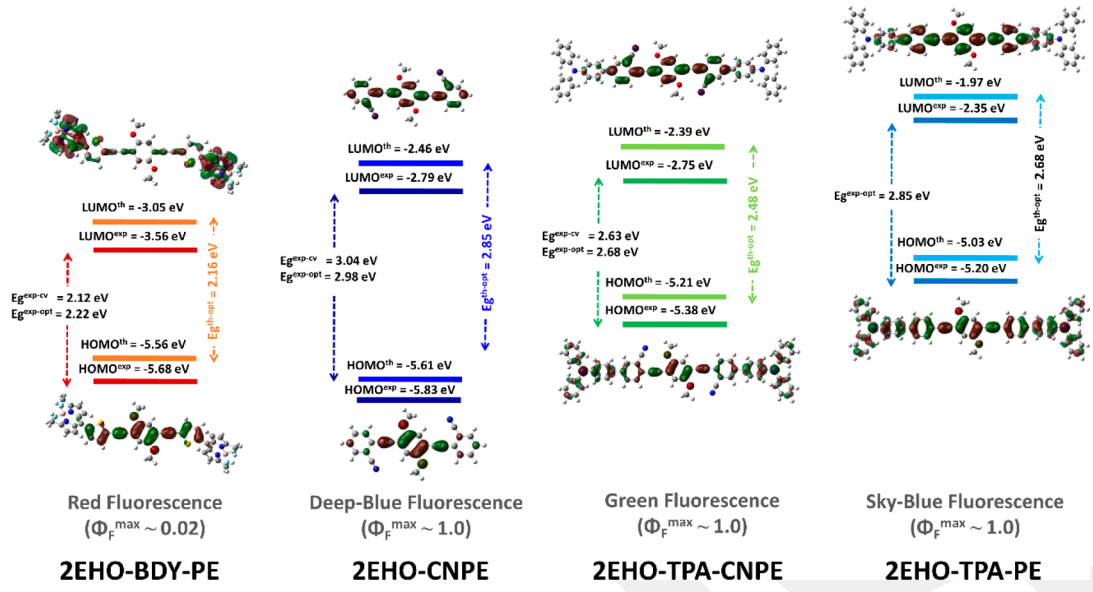

Figure 2. Energy diagrams showing theoretically calculated (light colors) and experimentally estimated (dark colors) HOMO/LUMO energy levels, frontier orbital topographies, and optical/electrochemical/theoretical band gaps for nonemissive **2EHO-BDY-PE**, deep blue emissive **2EHO-CNPE**, and green emissive **2EHO-TPA-CNPE** molecules developed in our earlier studies[35,36] and the new sky blue emissive **2EHO-TPA-PE** molecule developed in this study.

Scheme 1. Synthesis Route for Sky-Blue Emissive Molecule 4′,4‴-((2,5-Bis((2-ethylhexyl)oxy)-1,4-phenylene)bis(ethyne-2,1-diyl))bis(*N*,*N*-diphenyl-[1,1′-biphenyl]-4-amine) (2EHO-TPA-PE)

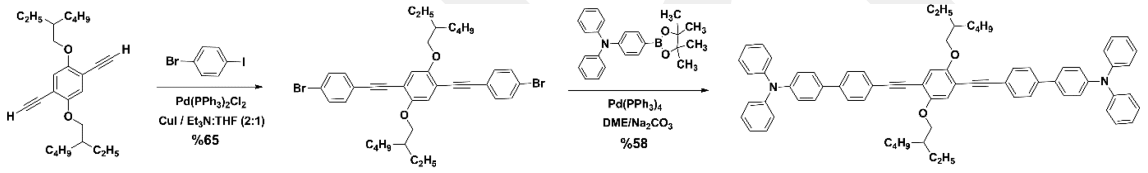

excited state character. It is noteworthy that, different from our first TPA-ended molecule, the removal of cyano units in the new molecule is very likely to optimize the CT characteristics in high polarity region with regards to quantum yield and lifetime. With the development of the new sky blue emissive molecule, a molecular library would be formed to systematically elucidate the relationships of molecular design−electronic structure−exciton characteristics in OPEs.

Based on presynthesis quantum mechanical modeling ((TD)-DFT, B3LYP/6-311G**), the theoretical frontier orbital energies are calculated to be −5.03 eV (for HOMO) and −1.97 eV (for LUMO) for the new molecule (Figure 2). When compared with the green emissive **TPA-2EHO-CNPE**, the absence of the cyano groups resulted in higher HOMO/LUMO energies for **TPA-2EHO-PE** with a larger energetic destabilization in LUMO (ΔE_{LUMO} = 0.42 eV vs. ΔE_{HOMO} = 0.18 eV). This is because there is a wave function density on the cyano groups in **TPA-2EHO-CNPE**'s LUMO topography, while HOMOs are delocalized only along the OPE π-backbone (negative resonance effect $(-R)$) ≫ negative inductive effect $(-I)$).[43−45] The calculated absorption spectrum for the new molecule shows that the $S_0 \rightarrow S_1$ electronic transition (HOMO → LUMO; f = 2.87) occurs at 2.68 eV (λ= 463 nm) (Figure S1), which is tuned to be between those of our previously reported deep blue and green emissive OPEs. This electronic structure is very likely to produce a sky blue fluorescence. These frontier orbital topographies, in which the HOMO is delocalized along the entire molecular π-system (D′−Ar−π−D−π−Ar−D′) and the LUMO is delocalized on the central Ar−π−D−π−Ar moiety, suggest that HLCT characteristics could be effectively utilized during electronic transitions. Interestingly, the HOMO−1 orbital is energetically very close to HOMO (ΔE = 0.17 eV), and it is purely localized on the TPA donor units (*vide infra*). Therefore, the involvement of HOMO−1 in electronic transitions is very likely, and it could induce a strong intramolecular charge transfer and a large excited state dipole from molecular termini to the central Ar−π−D−π−Ar unit. Therefore, we expect this new OPE molecular π-system to give a tunable CT-character depending on solvent polarity. These initial theoretical findings are found to be in great agreement with the experimental characterizations, and further insights were gained via detailed TDDFT studies (*vide infra*).

The new sky blue emissive molecule was synthesized in 58% yield by a Suzuki cross-coupling reaction between triphenylamine pinacol boronic ester and **2EHO-Br-PE** in the presence of $Pd(PPh_3)_4$ catalyst and Na_2CO_3 base in dimethoxyethane (DME) as shown in Scheme 1. Prior to this final step, while the synthesis of **2EHO-DEB** was carried out in accordance with our previously reported procedure (see the Supporting Information for details), the intermediate compound **2EHO-Br-PE** was synthesized via a halogen-selective Sonogashira cross-coupling reaction between **2EHO-DEB** and 1-bromo-4-iodobenzene in 65% yield. This corresponds to ∼80% yield and a high selectivity for each iodo position. Despite the absence of electron-

https://doi.org/10.1021/acs.jpcb.1c07165
J. Phys. Chem. B 2021, 125, 11717−11731

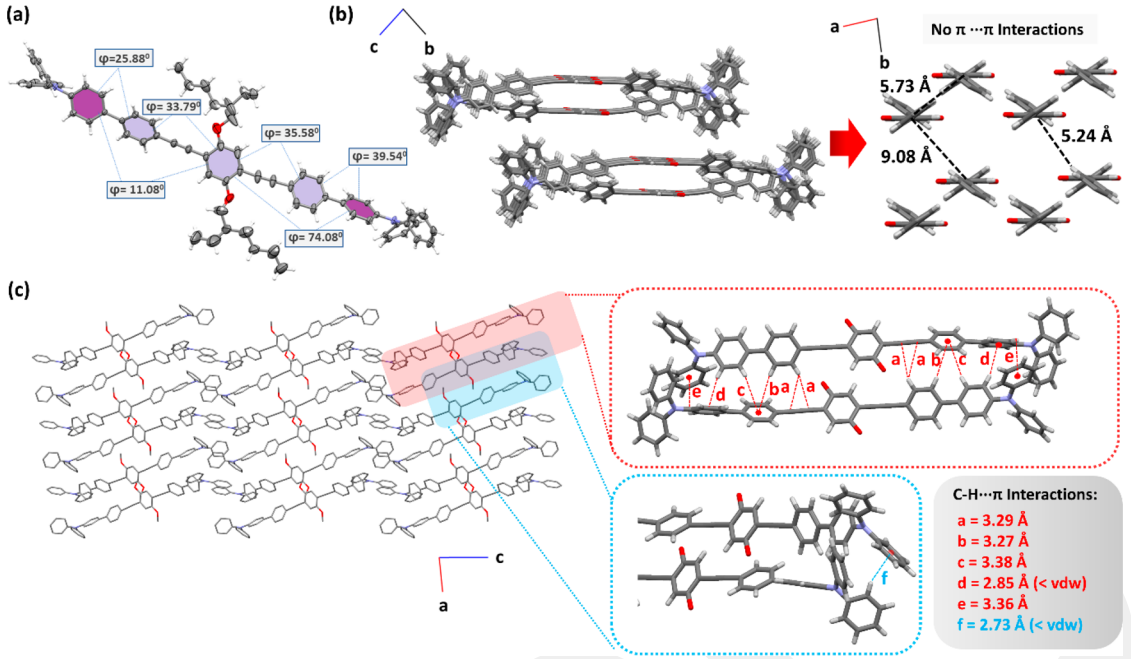

Figure 3. (a) ORTEP drawing of the molecular structure for **2EHO−TPA-PE** (20% probability level) showing the corresponding torsion angles and π-backbone coplanarity. Perspective views of the slipped π-stack arrangement viewed along the crystallographic *a*- and *c*-axes (b) and *b*-axis (c) showing large centroid-to-centroid distances (5.24/5.73/9.08 Å) with no evident $\pi-\pi$ interactions. Multiple strong "C−H···π" interactions (*a* = 3.29 Å, *b* = 3.27 Å, *c* = 3.38 Å, *d* = 2.85 Å (<vdw), *e* = 3.36 Å, and *f* = 2.73 Å (<vdw)) are identified along the slip direction. The flexible alkyl side chains (b and c) and the triphenylamine units (b, right panel) are omitted for clarity.

withdrawing cyano groups, this selectivity arises from the better reactivity of iodo substituent as compared to the bromo one, which facilitates the rate-determining oxidative addition step in the catalytic cycle.[46,47] The final compound showed great solubility in common organic solvents and was purified via column chromatography on silica gel using CH_2Cl_2:hexanes (3:1, v/v) solvent mixture. The chemical structures/purities were confirmed by a series of characterizations including ^1H and ^{13}C NMR spectroscopies, MALDI−TOF mass spectrometry, elemental analysis, and thin-layer chromatography (Figures S2−S8).

The thermal properties of the new molecule were examined by differential scanning calorimetry (DSC) and thermogravimetric analysis (TGA). As shown in Figure S9, differential scanning calorimetry (DSC) characterization of **2EHO-TPA-PE** solid showed a high glass transition (T_g) temperature of 140 °C followed by a sharp endothermic peak at 164.7 °C (enthalpy of 25.72 J/g). As confirmed by a conventional melting point apparatus, the endothermic peak corresponds to the melting point (T_{mp} = 164−165 °C). When the isotropic liquid phase of **2EHO-TPA-PE** was cooled from 200 °C to room temperature, no crystallization peak was observed, and the melting peak disappeared in the successive heating giving only a glass transition (T_g = 140 °C). This indicates that the solvent removal after the chromatography yielded a semicrystalline solid (i.e., crystalline and amorphous domains coexist), which transformed into a glassy, amorphous state upon the first heating−cooling cycle. The observed glassy, amorphous state of **2EHO-TPA-PE** solid, when combined with its fluorescent properties, could be quite attractive for electroluminescent thin-film devices, and is consistent with those of previously reported arylamine terminated π-conjugated small molecules.[48−51] Thermogravimetric analysis (TGA) of the new molecule showed a thermolysis onset temperature (T_{onset}, 5% weight loss) of 315 °C indicating an excellent thermal stability (Figure S9). When T_{onset} and T_{mp} values are compared between **2EHO-TPA-PE** and **2EHO-TPA-CNPE** having the same extended OPE π-system, the presence of electron-withdrawing CN groups clearly increases thermal stability and intermolecular interactions (i.e., cohesive energetics) in the solid-state. Interestingly, regardless of their exact π-architectures and acceptor/aryl units, all four OPE small molecules shown in Figure 1 did not show any crystallization behavior during thermal cooling; these molecules tend to form crystallites only from solution during solvent removal.

Single-Crystal Structure and Intermolecular Interactions. In order to gain more insights into the molecular structure, solid-state packing, and intermolecular interactions for the new fluorescent molecule, clear yellow needle-like single-crystals were grown by diffusion of hexanes into an acetonitrile solution at room temperature, and were characterized by X-ray diffraction analysis (Figure 3). **2EHO-TPA-PE** crystallizes in the triclinic space group $P\bar{1}$, showing a slipped π-stack arrangement along the crystallographic *a*-axis (Figure 3c). As shown in Figure 3a, the π-backbone of the new molecule shows a distorted bowl-shaped structure with a large degree of nonplanarity. Unsymmetrical inter-ring torsions were observed along the molecular axis showing different dihedral angles on two different sides of the molecule making one side more coplanar compared to the other one. The dihedral angles between the phenyl rings were measured to be as high as 74.1°. The presence of swallow-tailed $-OCH_2CH(C_2H_5)C_4H_9$ alkyl substituents on the central benzene ring, along with the highly distorted π-backbone, were found to prevent efficient cofacial $\pi-\pi$ interactions in the crystal structure. Large centroid-to-centroid distances of 5.24/5.73/9.08 Å were measured between the "Ar−π−D−π−Ar" moiety of the neighboring molecules (Figure 3b). This finding matches well with the single-crystal

https://doi.org/10.1021/acs.jpcb.1c07165
J. Phys. Chem. B 2021, 125, 11717−11731

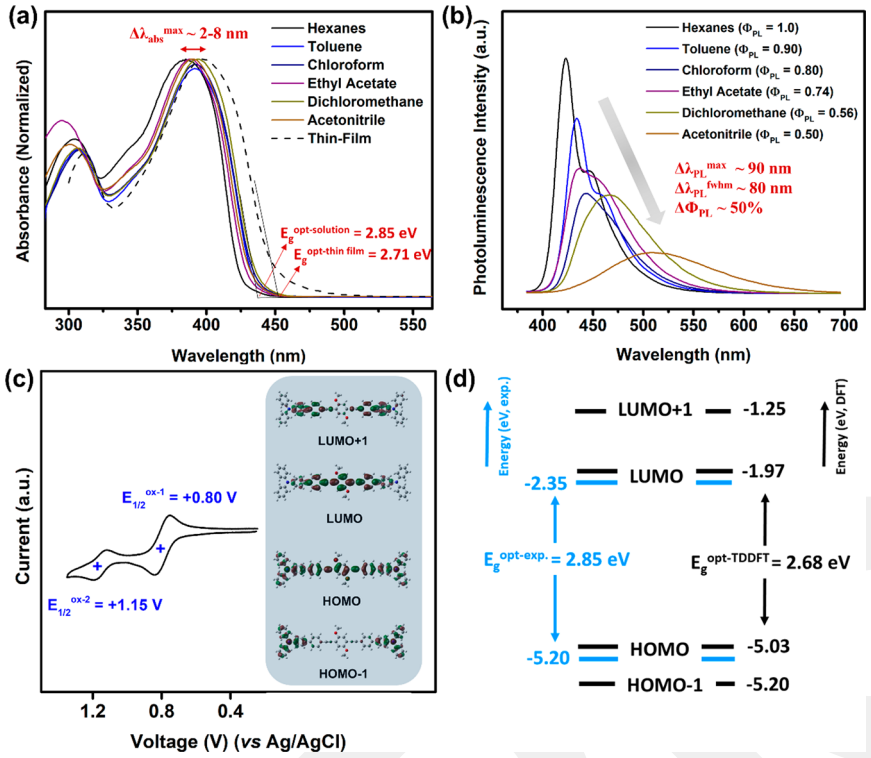

Figure 4. Solvatochromic optical absorption (1.0×10^{-5} M) (a) and photoluminescence (1.0×10^{-7} M) (b) spectra of **2EHO-TPA-PE** in six selected solvents with increased orientational polarizabilities (hexanes ($f(\varepsilon, \eta) = 0.001$) → acetonitrile ($f(\varepsilon, \eta) = 0.305$). The corresponding changes in the spectral characteristics with increased solvent polarity are indicated, and the optical band gap is calculated in hexanes. The optical absorption spectrum (dashed line) and the corresponding optical band gap are also shown for the spin-coated thin-film. (c) Cyclic voltammogram of **2EHO-TPA-PE** showing two reversible oxidation peaks in a 0.1 M (TBA)PF_6/CH_2Cl_2 solution vs. Ag/AgCl (3.0 M NaCl) at a scan rate of 50 mV s^{-1}. Inset shows the calculated frontier orbital topographies. (d) Experimental (sky blue lines) and theoretical (black lines) frontier orbital energy levels and optical/theoretical band gaps.

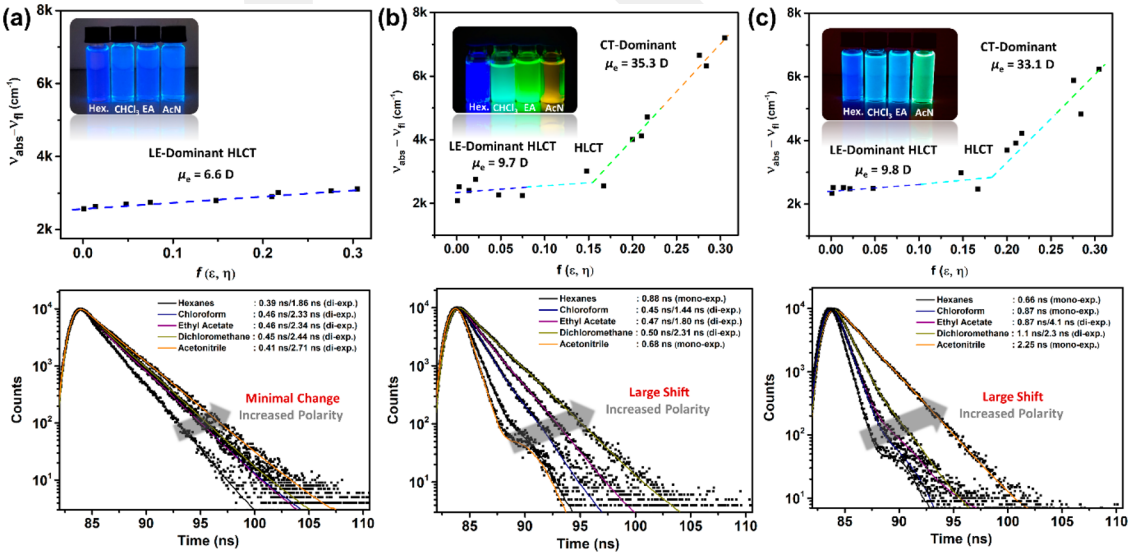

Figure 5. Solvatochromic Lippert−Mataga model of **2EHO-CNPE** (a), **2EHO-TPA-CNPE** (b), and **2EHO-TPA-PE** (c) showing the fitted linear correlations (Stokes shifts ($\nu_{abs} - \nu_{fl}$) against $f(\varepsilon, \eta)$), and the LE-dominant HLCT, HLCT, and CT-dominant excitonic regions. Insets show the optical images of molecular solutions in different solvents under optical excitation. The corresponding transient photoluminescence decay profiles for each molecule are measured under nitrogen atmosphere in different solvents (concentration = 1×10^{-7} M) at the fluorescence maxima upon excitation at 390 nm, and the mono/biexponential fitting curves with decay lifetimes are shown.

structure of our previously reported deep-blue emissive OPE molecule, **2EHO-CNPE**, that also showed minimum distances of 7.73 Å between the π-layers.[35] However, in the unit cell, two molecules were found to adopt a dimeric form by putting their relatively coplanar half in close contact with the relatively distorted half, which yields multiple very favorable intermolecular (*phenylene*)C−H···π(*phenylene/ethynylene*) interactions (a = 3.29 Å, b = 3.27 Å, c = 3.38 Å, d = 2.85 Å (<r_{vdw}(H) +

https://doi.org/10.1021/acs.jpcb.1c07165
J. Phys. Chem. B 2021, 125, 11717−11731

r_{vdw}(C) = 2.90 Å),[52] and e = 3.36 Å) between the corresponding phenylene and ethynylene units. Also, going from one unit cell dimer to the next one, short (*phenylene*)C−H···π (*phenylene*) contacts (f = 2.73 Å < r_{vdw}(H) + r_{vdw}(C) = 2.90 Å)[52] were identified between the triphenylamine molecular termini. As shown in Figure 3c, these interactions are indeed enabled by the presence of intramolecular twists that directs each (*phenylene*)-C−H bond into a favorable position to interact with the phenylene/ethynylene unit of the adjacent molecule, which also helps to extend one-dimensional slipped stack π-network into a 3D crystal structure. The observed solid-state microstructure for the new molecule with multiple (14 interactions in the dimeric form) strong C−H···π interactions makes the π-structures and the crystal lattice very rigid and precludes possible vibronic pathways to fluorescence decay in the solid-state by reducing exciton-vibronic couplings.[53,54] On the other hand, short π−π interactions are typically linked to increased exciton−phonon couplings, resulting in unfavorable fluorescence decays in the solid-state.[55,56] Therefore, the absence of π−π interactions in our case, along with the presence of multiple strong C−H···π interactions, are expected to lead to high quantum efficiencies in the solid-state ($\Phi_{PL\text{-solid state}}$ = 0.80, *vide infra*).[57] When the solid-state packing and the photoluminescence quantum efficiency of the new molecule is compared with those of our previously reported **2EHO-CNPE**, we see that **2EHO-CNPE** shows a much reduced $\Phi_{PL\text{-solid state}}$ of 0.50 associated with a significantly reduced degree of intermolecular C−H···π interactions.[35]

Photophysical/Electrochemical Properties and Solvatochromic Effect. As depicted in Figure 4, the initial molecular optoelectronic properties of the new sky blue emissive compound were obtained by UV−vis optical absorption and steady-state photoluminescence/transient photoluminescence decay spectroscopies and cyclic voltammetry. In order to obtain accurate information about the π-system without any charge-transfer state contribution, both absorption and emission profiles were recorded in hexanes as a nonpolar solvent. While the absorption maximum (λ_{abs}^{max}) corresponding to π−π* ($S_0 \rightarrow S_1$) transition of the molecular backbone was seen at 384 nm, the photoluminescence spectrum shows an emission peak maximum (λ_{PL}^{max}) at 422 nm. The photoluminescence quantum efficiency was measured to be unity (Φ_{PL} = 1.0). The transient photoluminescence decay profile in hexanes collected at 422 nm (λ_{exc} = 390 nm) showed a single-exponential decay with a very short lifetime of 0.66 ns (Figure 5c). This indicates a very efficient radiative $S_1 \rightarrow S_0$ electronic transition ($k_r = 1.51 \times 10^9$ s^{-1}) on the molecular π-backbone with minimal nonradiative losses. The optical band gap is measured as 2.85 eV from the low-energy absorption band edge. The optical absorption spectrum in solution correlates well with the TDDFT-calculated spectrum (Figure S1) with matching optical band gap value of 2.68 eV ($S_0 \rightarrow S_1$: HOMO → LUMO; f = 2.87). Going from solution to solid-state, λ_{abs}^{max} shifts to 397 nm and the optical band gap becomes 2.71 eV. As shown in Figure 4c, cyclic voltammetry characterization reveals two reversible oxidation peaks at +0.80 and +1.15 V, from which the HOMO/LUMO energies are estimated to be −5.20 eV/−2.35 eV. When compared with those of **2EHO-BDY-PE**, **2EHO-CNPE**, and **2EHO-TPA-CNPE**, the HOMO/LUMO energies of the new molecule are higher reflecting the structural changes of π-extension via TPA donors and removal of an acceptor unit in the new molecule. This finding is also in great agreement with the theoretical results and orbital topographies (Figures 2 and 4c,d). The solvatochromic ground and excited state characteristics of the new sky blue emissive molecule were revealed by studying optical absorption and photoluminescence (steady-state and time-resolved methods) spectra in 13 different solvents with varied orientational polarizabilities (hexanes ($f(\varepsilon,\eta)$ = 0.001) → acetonitrile ($f(\varepsilon,\eta)$ = 0.305). As shown in Figures 4a, 4b, and S10, although the UV−vis absorption spectra showed small changes ($\Delta\lambda_{abs}^{max} \sim 2-8$ nm) with increased solvent polarity, a strong solvatochromism was seen in the photoluminescence characteristics with substantial spectral changes of bathochromic shifts ($\Delta\lambda_{PL}^{max} \sim 90$ nm), increased full width at half-maximum values ($\Delta\lambda_{PL}^{fwhm} \sim 80$ nm), and lowered quantum yields ($\Delta\Phi_{PL} \sim 50\%$). In addition, the effect of solvent polarity on the exciton decay dynamics was evident in the time-resolved PL lifetime measurements (Figure 5). The complete spectral data depending on the solvent polarity is provided on Table S2. Based on these findings, it is evident that while the ground state (S_0) of **2EHO-TPA-PE** is not of any CT character, the radiative excited state (S_1) possesses a significant dipole moment as a result of intramolecular charge-transfer (CT) occurred upon photoexcitation. However, the effect of solvent polarity on the excited state characteristics of **2EHO-TPA-PE** π-system was found to be quite different in low-to-medium and high polarity regions. When the Lippert−Mataga model (Stokes shifts ($\nu_{abs} - \nu_{fl}$) against $f(\varepsilon,\eta)$) was applied for the solvent orientational polarizability ($f(\varepsilon,\eta)$) range of 0.001−0.305 (see Supporting Information for the model details), a two-section linear fitting (Figure 5c) was obtained indicating the two different excited state behaviors in low-to-medium and high polarity solvent regions. Using these linear fitting slopes and the DFT-calculated ground state dipole moment (μ_g = 0.0038 D), the excited state dipole moments (μ_e) of the S_1 state were estimated as 9.8 and 33.1 D in the low-to-medium and high polarity regions, respectively. In low-to-medium polarity region, the excited state of the new sky blue emissive molecule shows a LE-dominant HLCT character, which was evident not only from the relatively low μ_e value but also from high quantum yields ($\Phi_{PL} \sim 0.8-1.0$) with relatively small Stokes shift (λ_{PL}^{Stokes} = 38 nm in hexanes) and full width at half-maxima values ($\lambda_{PL}^{fwhm} \sim$ 25−40 nm in hexanes). Also, a vibronic structured emission profile was seen in low-to-medium polarity solvents with peak intervals of ∼1400−1600 cm^{-1} (aromatic C=C bond stretches) as an indicator of the LE-dominant excited state.[22,58] The vibronic character of the photoluminescence observed in the low-polarity solvents was also evident in the lifetime measurements that both (i.e., the main and vibronic) PL peaks (λ_{PL} = 422 and 448 nm in hexanes) gave exactly the same lifetime (τ = 0.66 ns in hexanes). Going to the high-polarity region, the vibronic structured emission profile completely disappears, the photoluminescence peak shows further bathochromic shift (λ_{PL}^{Stokes} = 126 nm in acetonitrile) and broadening (λ_{PL}^{fwhm} = 125 nm), and the quantum efficiency decreases by 50% (Φ_{PL} = 0.50 in acetonitrile). These changes reflect that the CT-character becomes dominant in the lowest-lying excited states of **2EHO-TPA-PE** in the high-polarity region. As shown in Figure S11, in the medium polarity region (i.e., ethyl acetate ($f(\varepsilon,n)$ = 0.200) and tetrahydrofuran ($f(\varepsilon,n)$ = 0.210)), a second lower-energy fluorescence starts to contribute to the photoluminescence process with a nearly equivalent intensity to the higher-energy one. Similar PL behaviors in the medium-polarity region were previously seen in a TPA-1,2-diphenyl-1*H*-phenanthro[9,10-d]imidazole (PPI) HLCT molecule.[22] Both of these emissions are shifted relative to the LE-dominant and CT-dominant emissions observed in hexanes and

https://doi.org/10.1021/acs.jpcb.1c07165
J. Phys. Chem. B 2021, 125, 11717−11731

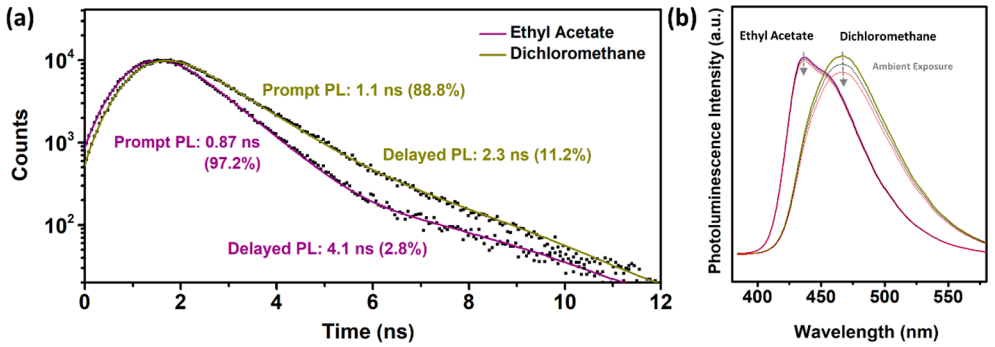

Figure 6. (a) Transient photoluminescence decay curves of **2EHO-TPA-PE** measured under nitrogen atmosphere in ethyl acetate ($f(\varepsilon,n) = 0.200$) and dichloromethane ($f(\varepsilon,n) = 0.217$) (concentrations = 1×10^{-7} M) at the corresponding fluorescence maxima upon excitation at 390 nm. The biexponential fitting curves with prompt/delayed decay lifetimes and contributions are shown. (b) Gradual decrease in the PL intensities when the same solutions are exposed to ambient atmosphere.

acetonitrile, respectively, and they are energetically very close ($\Delta\lambda_{PL}^{max} \sim 0.1$ eV). This points to the beginning of an effective hybridization between LE-dominant and CT-dominant states in the medium-polarity region, which completely turns into one broad ($\lambda_{PL}^{fwhm} \sim 85$ nm) emission peak once the proper solvent polarity and dielectric properties are met in dichloromethane ($f(\varepsilon,n) = 0.217$) (Figure S11).

Tunable Excited States and Interplay between Local Excited and Charge Transfer Characteristics. Solvent polarity-dependent excitonic behaviors of three emissive HLCT-OPE molecules are studied based on the Lippert−Mataga model. Here, we note that since **2EHO-BDY-PE** exhibits extremely weak fluorescence properties ($\Phi_{PL} \sim 0.02$, Figure S12), the same analysis could not be performed with this molecule. As shown in Figure 6, all three OPE molecules exhibit the common LE-dominant HLCT excited state characteristics in the low-to-medium polarity region ($f(\varepsilon, \eta) = 0-0.15$) with calculated excited state dipole moments (μ_e) of 6.6−9.8 D. In addition, for all three molecules, the quantum yields are very high ($\Phi_{PL} = 0.8-1.0$) while the Stokes shifts are small and the lifetimes are short ($\tau = 0.5-2.0$ ns) in this region as a result of the LE-dominant excited state character. However, going to high polarity region ($f(\varepsilon, \eta) > 0.2$), the presence of the triphenylamine donors and acceptor units, and the extent of the OPE π-system were found to have a significant effect to define the CT character of the excited state. While **2EHO-CNPE** retains the LE-dominated HLCT behavior in this high polarity region, **2EHO-TPA-CNPE** and **2EHO-TPA-PE** OPE π-systems showed much larger slopes (~27 170−29 700) in the Lippert−Mattaga model yielding very large μ_e's of 33.1−35.3 D. Note that these significantly large μ_e values are on the order of some of the highest excited state dipole moments predicted for CT compounds in the literature.[59,60] Considering that **2EHO-TPA-PE** and **2EHO-TPA-CNPE** molecular lengths are ~3.55 nm, these μ_e's correspond to a large degree of charge separation (~0.70−0.75 charge·nm) along the molecular π-backbone. These findings reveal that in low-to-medium polarity region there is a common LE-dominant HLCT excited state character for all three OPE molecules. While the LE-dominant HLCT character of the **2EHO-CNPE** spans the whole polarity range without inducing a strong CT-character, for π-extended **2EHO-TPA-PE** and **2EHO-TPA-CNPE** systems, HLCT and CT-dominant excitonic behaviors were evident in the medium and high polarity regions, respectively. This is a direct result of intramolecular charge transfer in the medium-to-high polarity region, which is facilitated with the addition of π-electron rich TPA donors with lone pairs and twistable aryl rings giving larger π-polarizability and higher degrees of rotational freedom to the OPE π-system. On the basis of TDDFT calculations (*vide infra*), these features are found to be crucial for an effective mixing of LE and CT states. However, a unique difference was observed between the CT characters of the **2EHO-TPA-PE** and **2EHO-TPA-CNPE** molecules. While **2EHO-TPA-PE** still exhibits a high PL quantum yield of 0.50 with a relatively long τ of 2.25 ns in acetonitrile, the same π-system with electron-withdrawing cyano (−CN) substituents (i.e., **2EHO-TPA-CNPE**) shows a much lower PL quantum yield of 0.15 (Figure S13) with a short τ of 0.68 ns. When nonradiative transition rates were compared for these two molecules, much higher k_{nr} value of 1.25×10^9 s^{-1} was measured in **2EHO-TPA-CNPE** as compared to that of **2EHO-TPA-PE** ($k_{nr} = 2.2 \times 10^8$ s^{-1}). Considering that both molecules have exactly the same OPE π-backbone, it is apparent that the presence of the electron-withdrawing cyano groups gives a strong nonradiative character to the intramolecular charge transfer excited state in **2EHO-TPA-CNPE** that largely quenches fluorescence. The π-system of the new sky blue emissive molecule appears to yield a tuned CT-dominance in the excited state, which still shows good fluorescence emission as a result of competitive k_r (2.2×10^8 s^{-1}) and k_{nr} (2.2×10^8 s^{-1}) values. This CT-effect was observed to be very weak in **2EHO-CNPE**—despite the presence of cyano substituents—when TPAs are removed; a high quantum yield of ~0.7−0.8 was measured for **2EHO-CNPE** even in high polarity solvents (i.e., acetone and acetonitrile) with small Stokes shifts (~10−12 nm) (Figure S13).

The degree of CT contribution in the excited state was found to have a profound effect on the radiative transition rates (k_r's). Especially, for TPA-ended molecules **2EHO-TPA-PE** and **2EHO-TPA-CNPE**, k_r values were found to be decreased (×5−7) in acetonitrile ($k_r = (2.0-2.2) \times 10^8$ s^{-1}) as compared to those measured in hexanes ($k_r = (1.2-1.4) \times 10^9$ s^{-1}). In solvents between hexanes and acetonitrile with medium polarities, the k_r values were found to gradually decrease as a result of the corresponding gradual changes in τ and Φ_{PL} values. However, the effect of CT-contribution to the radiative transition rate (k_r) was not as profound in **2EHO-CNPE**, and wide range of solvent polarities yield only a small change in k_r values ($k_r = (4.0-5.0) \times 10^8$ s^{-1}). TPA-ended molecules **2EHO-TPA-PE** and **2EHO-TPA-CNPE** showed ×2−3 larger k_r values as compared to **2EHO-CNPE** in nonpolar solvents, which correlate perfectly with the calculated oscillator strengths for $S_1 \rightarrow S_0$ transitions ($f = 2.7/3.3$ for **2EHO-TPA-CNPE**/**2EHO-**

https://doi.org/10.1021/acs.jpcb.1c07165
J. Phys. Chem. B 2021, 125, 11717−11731

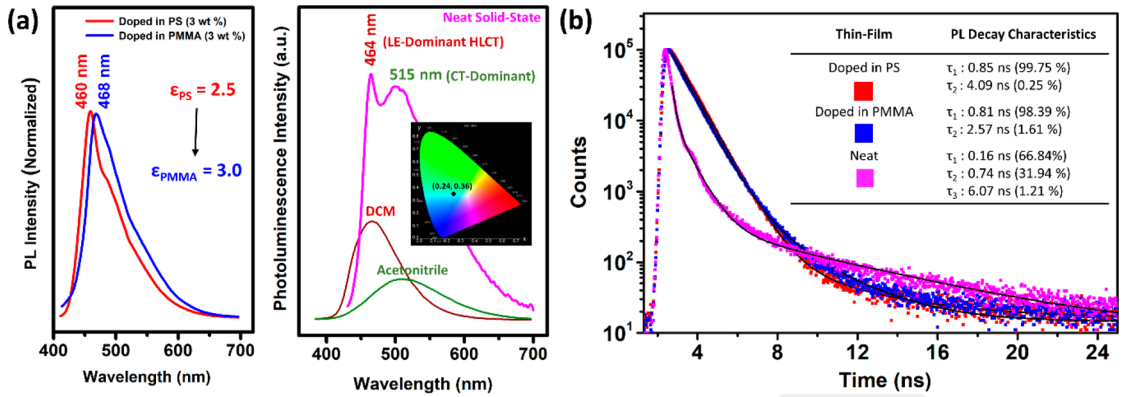

Figure 7. (a) Photoluminescence spectra of **2EHO-TPA-PE** as doped (3 wt %) molecule in polystyrene (PS) and poly(methyl methacrylate) (PMMA) polymer matrices, and as spin-coated neat thin-film. Inset on the right shows CIE 1931 chromaticity diagram showing the sky blue emission (x, y) coordinates. (b) Transient photoluminescence decay curves of **2EHO-TPA-PE** thin-films at the corresponding fluorescence maxima upon excitation at 390 nm. The exponential fitting curves with prompt/delayed decay lifetimes and contributions are shown.

TPA-PE vs. f = 1.1 for **2EHO-CNPE**). This is a direct result of extended π-systems and increased hole-particle orbital wave function overlaps in **2EHO-TPA-PE** and **2EHO-TPA-CNPE**.

Consistent with the Lippert−Mataga model analysis showing a single-stage LE-dominant HLCT excitonic behavior (Figure 5a), **2EHO-CNPE**'s exciton dynamics in PL decay profiles were minimally affected from solvent polarity. However, for TPA-ended molecules **2EHO-TPA-PE** and **2EHO-TPA-CNPE**, PL decay profiles showed substantial changes, especially going to higher polarities (Figure 5, parts b and c). For all three molecules, upon meeting the proper solvent polarity, which is mostly medium polarity solvents, a biexponential decay profile was observed with the delayed fluorescence lifetimes of ∼2−4 ns (3−11% contributions to the whole process) whereas the prompt decays showed ∼0.4−0.9 ns lifetimes. This is ascribed to fluorescence delayed through R(ISC) processes between S_1 and T_m ($m > 1$) states, and similar nanoscale lifetimes were predicted in the literature for a few R(ISC) processes.[9,58] As shown in Figure 6a, going from ethyl acetate ($f(\varepsilon,n)$ = 0.200) to dichloromethane ($f(\varepsilon,n)$ = 0.217), the contribution of the delayed process to fluorescence was found to increase from 2.82% to 11.20%, and the delayed lifetime decreased from 4.1 to 2.3 ns (i.e., increased $k_{R(ISC)}$), which indicates a more favorable R(ISC). As a further confirmation that high-lying triplet states are populated during photoexcitation, lowered PL intensities (Figure 6b) were recorded when nitrogen flushed solutions in medium-polarity solvents were exposed to ambient atmosphere. And, consistent with the solvent difference in the PL decay profiles, the decrease in PL intensity upon ambient exposure for dichloromethane is greater than that of ethyl acetate. This suggests that, in the medium polarity region, even small changes in the solvent medium could induce strong effects on the R(ISC) processes, and dichloromethane appears to offer an ideal polarity and dielectric properties. At this point, it is important to note that in the medium polarity region, while most solvents give two-equal-intensity-peak emission profiles, dichloromethane yielded a single broad emission peak (Figure S11), as a result of favorable LE and CT states hybridization (*vide infra*). This is also the key reason for the above-mentioned increased (R)ISC efficiency in dichloromethane.

In order to understand whether the polarity-dependent excitonic behavior in solvent medium could be translated into solid-state, **2EHO-TPA-PE** doped thin-films (3 wt %) were prepared on glass using polystyrene (PS) and poly(methyl methacrylate) (PMMA) polymeric matrices, as well as neat molecular thin-film for comparison. As shown in Figure 7a, consistent with the fluorescence properties in medium-polarity solvents and the increased dielectric constant going from PS to PMMA ($\varepsilon_{polymer}$ = 2.5 → 3.0), while the PS-doped film showed λ_{PL}^{max} at 460 nm, PMMA-doped film showed a red-shifted fluorescence with a maximum at 468 nm. On the other hand, going to neat molecular solid-state, since the dielectric constant of most π-systems corresponds to medium-polarity solvents (e.g., dichloromethane ($f(\varepsilon,n)$ = 0.217)) λ_{PL}^{max} appears at 464 nm (Figure 7b). In addition, a broad lower energy emission peak (λ_{PL}^{max} = 515 nm) was also seen in the neat thin-film, which carries the features of those observed in high polarity solvents (acetonitrile: $f(\varepsilon,n)$ ∼ 0.3). The coexistence of LE-dominant HLCT and CT-dominant excited state characteristics at the same time is different than solutions, and it is clearly a result of enhanced intermolecular π-interactions in the solid-state as evidenced from the single-crystal structure (*vide supra*, Figure 3). The Commission Internationale de l'Eclairage (CIE) (x, y) coordinates of the neat thin-film are determined to be (0.24, 0.36), which corresponds to a sky blue emission. The solid-state quantum efficiencies for both neat thin-film and single-crystal were measured to be very high ($\Phi_{PL\text{-solid state}}$ ∼ 0.78 and 0.81, respectively) using an integrating sphere method. The observed high solid-state quantum yield in the single-crystal is consistent with the presence of multiple strong C−H···π interactions and the absence of π−π interactions in the crystal lattice (*vide supra*), both of which prevents unfavorable fluorescence decays via exciton-vibronic/phonon couplings.[53] Here, we note that similar short-range interactions were also evident in the XRD characterization (a broad peak with 2θ = 16−29° in Figure S14) of the spin-coated neat thin-film, which apparently contributes to the observed high fluorescence efficiency in thin-film phase even though long-range ordering is not present. As shown in Figure 7b, **2EHO-TPA-PE**-doped PS and PMMA thin-films showed very similar decay profiles to those observed in the medium-polarity solvents with major prompt decays (0.85 ns (99.75%) and 0.81 ns (98.39%), respectively) followed by minor delayed decay channels (4.09 ns (0.25%) and 2.57 ns (1.61%), respectively). Remarkably, the aforementioned concurrent changes of decreased $\tau_{delayed}$ and increased delayed contribution in the medium-polarity solvent range (for ethyl acetate → dichloromethane) were also observed in the solid-state going from PS to PMMA. In the exciton decay profile of the **2EHO-**

https://doi.org/10.1021/acs.jpcb.1c07165
J. Phys. Chem. B 2021, 125, 11717−11731

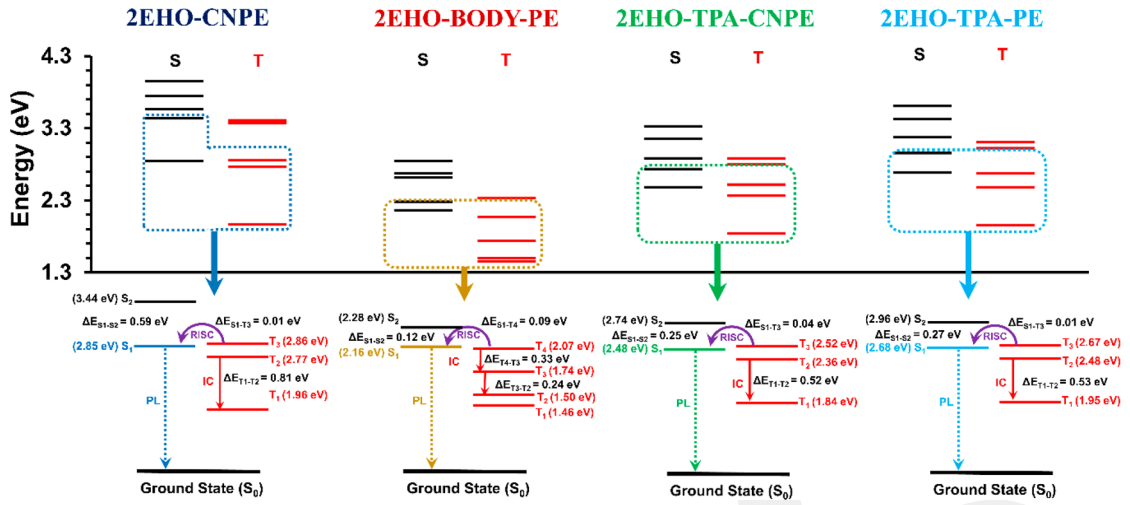

Figure 8. Calculated energies of the first 5 singlet (S) and triplet (T) excited states along with the illustration of possible exciton decay paths for the current OPE-based π systems.

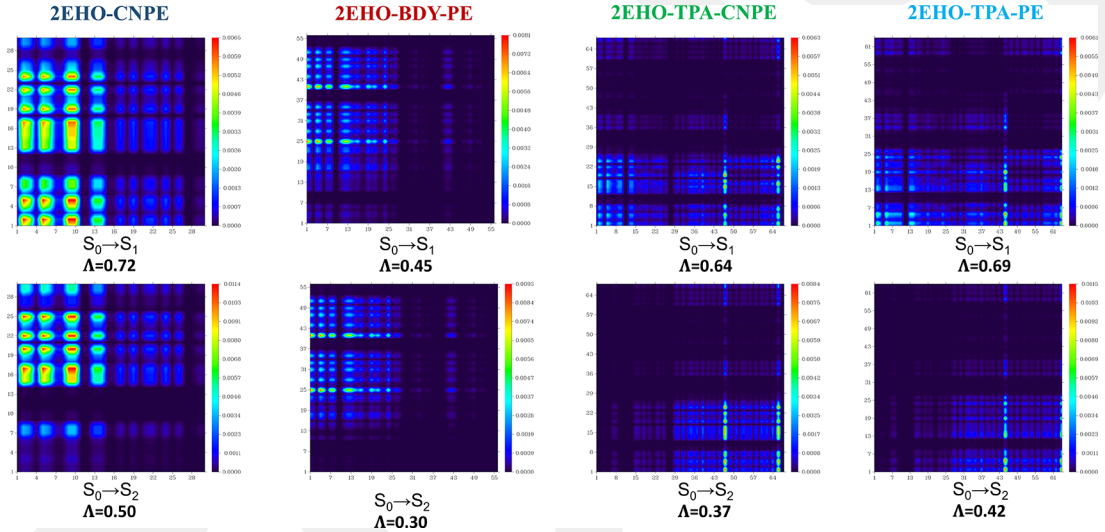

Figure 9. Calculated transition density maps (TDMs) and Λ values for the $S_0 \rightarrow S_1$ and $S_0 \rightarrow S_2$ transitions of the current OPE-based π systems. For TDMs, atomic indices start from the center of the molecule and increase toward the peripheral, and contributions from hydrogens are excluded.

TPA-PE neat thin-film, a unique triexponential decay behavior was seen, with the average lifetime of the prompt decays at 0.36 ns and the (R)ISC-delayed fluorescence lifetime at 6.07 ns.

Excited State Properties via TDDFT and Contribution of Triphenylamine Structural Flexibility to Hybridization. The excited state properties of the OPE-based π systems are further investigated using TDDFT methods at B3LYP/6-311** level of theory. In Figure 8, we show the excited state energetics for the first 5 singlet and triplet excited states along with the possible exciton-decay processes, whereas the hole and particle wave functions are shown in Figure S15. As discussed earlier in our previous reports, both **2EHO-CNPE** and **2EHO-TPA-CNPE** molecules are shown to facilitate RISC process upon photoexcitation. Their excited-state energy profiles exhibit sufficiently large energy gaps between T_1 and T_2 states ($\Delta E_{T_2\text{-}T_1}$ = 0.81 eV (for **2EHO-CNPE**) and 0.53 eV (for **2EHO-TPA-CNPE**)), which can limit $T_n \rightarrow T_1$ internal conversions (ICs). In addition, these molecules have very small $\Delta E_{S_1\text{-}T_n}$ ($\Delta E_{S_1\text{-}T_3}$ = 0.01−0.04 eV) that can enhance the rate of RISC process from higher-lying triplet states to S_1 state. In the case of **2EHO-TPA-PE**, both singlet and triplet excited state energies show a considerable blue-shift compared to those of **2EHO-TPA-CNPE** as a result of its D′−Ar−π−D−π−Ar−D′ architecture without an acceptor unit (Figure 1). On the other hand, hole and particle wave functions of **2EHO-TPA-PE** and **2EHO-TPA-CNPE** (Figure S15) exhibit a similar topography except for the contribution from cyano groups on the particle wave functions of the latter. Among investigated systems, electronic structure and excited-state characteristics of **2EHO-BDY-PE** with its AA−π−D−π−AA architecture (Figure 1b) show a drastic deviation from the other OPE π systems. This is, of course, a result of the presence of strong BODIPY acceptor units which make significant contributions to LUMO/LUMO +1 and alter the electronic structure along with the nature of excited states. As shown in Figure 8, different than the other OPE π-systems, the excited-state energy profile of this molecule could potentially deteriorate RISC process since the $T_n \rightarrow T_1$ IC rate could be quite large due to energetically close triplet states ($\Delta E_{T_4\text{-}T_3}$ = 0.33 eV, $\Delta E_{T_3\text{-}T_2}$ = 0.24 eV and $\Delta E_{T_3\text{-}T_2}$ = 0.05 eV). In general, particle and hole wave functions of low-lying excited states for **2EHO-BDY-PE** show a significant increase in the CT

https://doi.org/10.1021/acs.jpcb.1c07165
J. Phys. Chem. B 2021, 125, 11717−11731

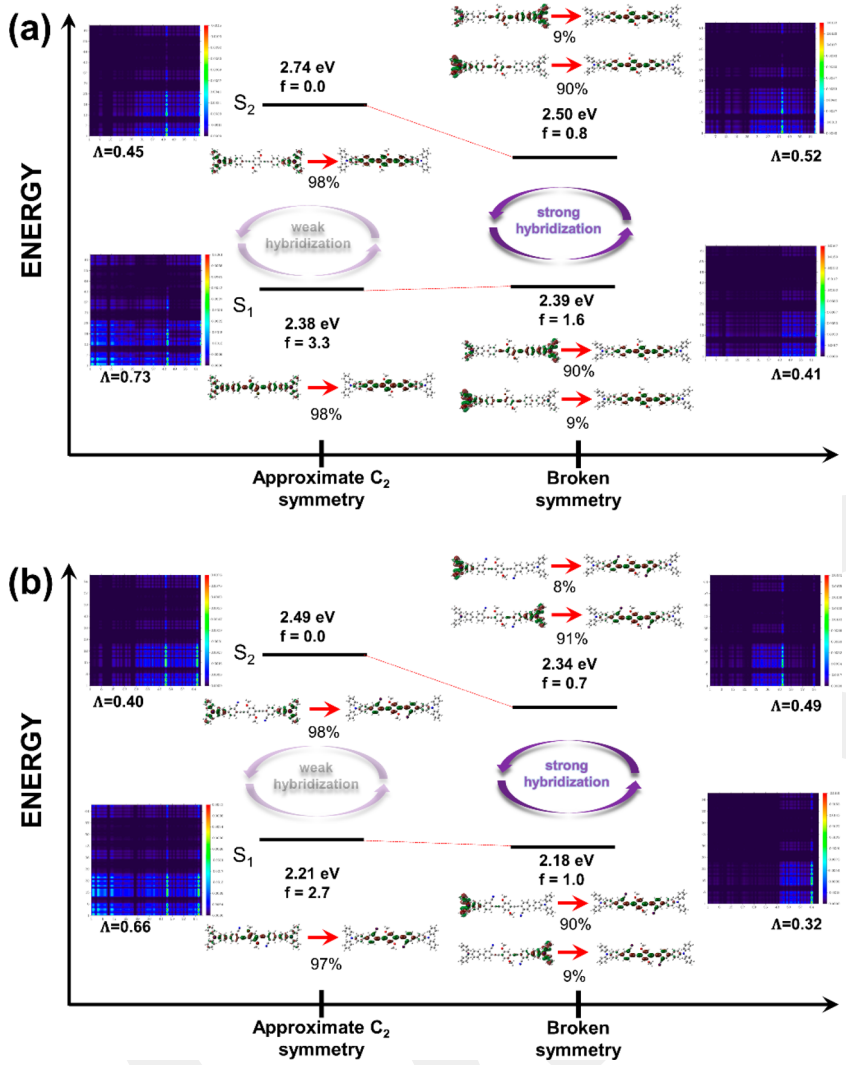

Figure 10. Illustration of the hybridizations between LE and CT states in the approximate-C_2 and the broken-symmetry geometries for the excited states of **2EHO-TPA-PE** (a) and **2EHO-TPA-CNPE** (b).

character compared to the other investigated OPE π systems. (Figure S15). Therefore, the oscillator strength of $S_0 \rightarrow S_1$ transition is predicted to be relatively low but nonvanishing (f = 0.89) for an extended π architecture. When the excited-state potential energy surface of S_1 state is explored with respect to the dihedral angle (φ) between the BODIPY moieties and the π−D−π core (Figure S16), it is very clear that this system exhibits the characteristics of twisted intramolecular charge transfer (TICT) state with a full charge separation at φ = 90°. In addition, the calculated total excited state energy of the **2EHO-BDY-PE**'s S_1 state generally shows a decrease with increasing φ, while the oscillator strength of $S_1 \rightarrow S_0$ transition approaches to zero, which is most likely the cause of weak fluorescence properties ($\Phi_{PL} \sim 0.02$, Figure S12) for this system.

As is evident from the solvatochromic shifts and the Lippert−Mataga curves (Figure 5), both **2EHO-TPA-PE** and **2EHO-TPA-CNPE** exhibit an interplay between LE and CT states upon photoexcitation whereas **2EHO-CNPE** does not. Previous theoretical analysis shows that, for effective formation of an HLCT state, LE and CT hybridization should contribute to both S_1 and S_2 states.[61] In that regard, we further explore the nature of these states using calculated transition density maps (TDMs), which shows the probability of finding electron and hole densities on individual atoms, along with the Λ values ($0 \leq \Lambda \leq 1$) that measure the spatial overlap between electron and hole wave functions. As shown in Figure 9, the $S_0 \rightarrow S_1$ transition of **2EHO-CNPE** shows LE-dominant HLCT character (Λ = 0.72) whereas the $S_0 \rightarrow S_2$ transition shows an increase in the CT character (Λ = 0.50), as expected from the NTO analysis (Figure S15). Introduction of TPA moieties to the OPE π-architecture results in an overall increase in the CT character for both $S_0 \rightarrow S_1$ (Λ = 0.64 and 0.69 for **2EHO-TPA-CNPE** and **2EHO-TPA-PE**, respectively) and $S_0 \rightarrow S_2$ transitions (Λ = 0.37 and 0.42 for **2EHO-TPA-CNPE** and **2EHO-TPA-PE**, respectively). For the $S_0 \rightarrow S_2$ transition, strong hole contributions from the TPA moieties essentially form a CT-dominant HLCT state with a vanishing oscillator strength. We also note that the energy gaps between S_1 and S_2 states (Figure 8) of **2EHO-TPA-CNPE** and **2EHO-TPA-PE** are considerably smaller compared to those in **2EHO-CNPE** (0.25−0.27 vs. 0.59 eV). As illustrated in Figure 1, these findings suggest that the interstate coupling between CT and LE states and the interplay of this coupling with respect to medium polarity is expected to be more pronounced for **TPA**-containing **2EHO-TPA-CNPE** and **2EHO-TPA-PE** when compared with **2EHO-CNPE**. In the case of **2EHO-BDY-PE**, however, both $S_0 \rightarrow S_1$ and $S_0 \rightarrow S_2$

https://doi.org/10.1021/acs.jpcb.1c07165
J. Phys. Chem. B 2021, 125, 11717−11731

transitions exhibit strong CT characters (Λ = 0.45 and 0.30), along with minimal hybridization from the LE state as a result of strong electron-acceptor units in the peripheral. These theoretical results are in excellent agreement with the previously discussed photophysical findings.

In addition to the immediate changes in the electronic structure and excited-state characteristics, outer TPA units in the architecture also provides the OPE π systems with several degrees of freedom for the geometry, especially through rotation on single (*phenyl*)C−C (*phenyl*) and (*phenyl*)C−N bonds. While all investigated OPE π systems exhibit an approximate C_2 symmetry for their S_0 and S_1 geometry, our test calculations showed that TPA-containing systems possess a relatively flat potential energy surface. As illustrated in the Lippert−Mataga curves, excited-state wave functions of the S_1 states undergo a large change from LE-dominant to HLCT and CT-dominant character upon polarity change, which is most likely accompanied by alterations in the geometry via coupling between electronic and nuclear motion. To investigate this effect on the excited states, geometry optimizations for the S_1 state have been performed for **2EHO-TPA-PE** and **2EHO-TPA-CNPE** starting from the approximate-C_2 geometry or the altered geometry with broken symmetry.

As shown in Figure 10, both systems' S_1 and S_2 states show a somewhat weaker hybridization of LE and CT states for the symmetric molecule, as the S_1 state exhibits strong LE character as indicated by the large Λ value and the oscillator strength, whereas the S_2 state shows a strong CT character with small Λ value and vanishing oscillator strength. In addition, configuration−interaction analysis shows that S_1 and S_2 states almost exclusively originate from HOMO → LUMO and HOMO−1 → LUMO transitions, respectively. In the broken symmetry cases, however, the energy gap between S_1 and S_2 states become smaller while the S_1 states gain CT character as indicated by the reduction in the Λ value as well as the oscillator strength, whereas the opposite occurs for the S_2 states. Furthermore, as a result of reduced symmetry, both HOMO → LUMO and HOMO−1 → LUMO configurations contribute to S_1 and S_2 states, indicating a stronger hybridization of LE and CT characters. We note that excited-state symmetry breaking has been reported previously for some molecules exhibiting similar π-architectures to **2EHO-TPA-CNPE** and **2EHO-TPA-PE**.[62−65] Moreover, it has been shown that excited-state symmetry breaking is mainly driven by solvent fluctuations in polar environments, which is also accompanied by increasing CT character, whereas in weakly polar media, solvent fluctuations cannot induce such an effect and the excited state remains mainly delocalized over the entire π-backbone.[62] This interaction picture is quite comparable to what was observed in the Lippert−Mataga curves (Figure 5) along with the excited state analysis in different geometries (Figure 10) for **2EHO-TPA-CNPE** and **2EHO-TPA-PE** molecules. Furthermore, the HLCT nature for S_1 and S_2 states of TPA-containing symmetric molecules has been previously demonstrated,[66−69] and it is likely that this HLCT character is not solely induced by the electron-donor ability of TPA moieties, but also facilitated by the geometric adaptability of such systems to symmetry-breaking and wave function hybridization for the lowest-lying excited states.

CONCLUSIONS

In summary, a new highly soluble sky blue emissive (CIE = 0.24, 0.36) oligo(*p*-phenyleneethynylene) (OPE) molecule, 4′,4‴-((2,5-bis((2-ethylhexyl)oxy)-1,4-phenylene)bis(ethyne-2,1-diyl))bis(*N*,*N*-diphenyl-[1,1′-biphenyl]-4-amine) (**2EHO-TPA-PE**) has been designed, synthesized, and its detailed structural, physicochemical, single-crystal, and optoelectronic characterizations have been performed in detail. The new molecule includes a D′−Ar−π−D−π−Ar−D′ molecular architecture with an extended π-spacer (ethnylene−phenylene) and no acceptor unit. Highly efficient fluorescence behavior in solution and solid-state ($\Phi_{PL\text{-}solution} \sim 1$ and $\Phi_{PL\text{-}solid\ state} \sim 0.8$) with a strong solvatochromism was observed. The absence of π−π interactions, along with the presence of multiple (14 interactions per dimeric form) strong C−H···π interactions, were revealed to lead to a high solid-state quantum efficiency as a result of suppressed exciton−phonon/vibronic couplings. The solvent or solid-state medium dipole-dependent excited state behavior covers a wide spectral region, and shows local excited (LE) → HLCT → charge transfer (CT) transition going from low-polarity to medium and high polarities. The CT state was observed to be highly fluorescent ($\Phi_{PL\text{-}high\ polarity} \sim 0.5$) despite extremely large Stokes shift (∼130 nm)/fwhm (∼125 nm) and significant charge separation (0.75 charge·nm). Herein, with the development of the new molecule, an HLCT OPE molecular library has been studied, for the first time in the literature, systematically via experiment and theory, and key relationships between molecular design−electronic structure−exciton characteristics were elucidated with regards to excited states and hot exciton channel formations. The addition of π-electron-rich TPA donors with lone pairs and twistable aryl rings gives a larger π-polarizability and higher degrees of rotational freedom to the OPE π-system, which is found to be critical for an effective/tunable mixing of LE and CT states. Accordingly, a unique relationship between excited-state symmetry breaking process and the formation of HLCT state is discussed for TPA-ended rod-shaped OPE π-systems. Introducing strong outer acceptor units (BODIPYs) through a C−C single bond (in **2EHO-BDY-PE**) results in an unfavorable excited state energy profile for hot-exciton harvesting as well as weak emissive properties as a result of twisted intramolecular charge-transfer. For all OPEs, (R)ISC-based delayed fluorescence processes ($\tau \sim 2$−6 ns) following the prompt decays (∼0.4−0.9 ns) were observed both in the solution and the solid-state, which could be finely tuned and facilitated via small dielectric changes in the medium. With the unique insights provided in our study into the structural/electronic factors governing tunable excited states and hot-exciton channel formations, rod-shaped oligo(*p*-phenyleneethynylene) stands out as a highly promising π-framework for the development of solution-processable luminescent materials. From an organic synthesis perspective, structurally varied fluorescent OPE molecules with a wide range of excited state and photophysical properties could easily be designed, synthesized, and studied in the near future. The excitonic properties (LE vs. HLCT vs. CT) of OPEs could be finely tuned and adjusted for a particular optoelectronic or sensing application by tuning the solution or solid-state medium dielectric properties and intermolecular interactions. In particular, the development of fluorescent molecules with HLCT excited states and (R)ISC channels could greatly benefit from the OPE π-framework for solution-processed (un)-conventional luminescence applications.

https://doi.org/10.1021/acs.jpcb.1c07165
J. Phys. Chem. B 2021, 125, 11717−11731

■ ASSOCIATED CONTENT

Supporting Information

The Supporting Information is available free of charge at https://pubs.acs.org/doi/10.1021/acs.jpcb.1c07165.

Calculated UV−vis absorption spectrum of **2EHO-TPA-PE** and the molecular orbitals involved in the low-lying excited states (Figure S1); synthesis of **2EHO-DEB** (Scheme S1); chemical characterizations (^{1}H NMR for intermediate compounds **1**, **2**, **2EHO-DEB**, and **2EHO-Br-PE** (Figures S2−S5) and ^{1}H/^{13}C NMR and MALDI TOF−MS spectra for **2EHO-TPA-PE** (Figures S6−S8)); crystal structure determination details and crystal data/refinement parameters for 2EHO-TPA-PE (Table S1); DSC and TGA curves of **2EHO-TPA-PE** (Figure S9); solvatochromic optical absorption/photoluminescence spectra of **2EHO-TPA-PE** in 13 different solvents (Figures S10 and S11); photoluminescence spectra of **2EHO-BDY-PE** (Figure S12); solvatochromic photoluminescence spectra of **2EHO-CNPE** and **2EHO-TPA-CNPE** in different solvents (Figure S13); $\theta-2\theta$ XRD pattern of the spin-coated **2EHO-TPA-PE** thin-film (Figure S14); solvatochromic Lippert−Mataga model details and data for **2EHO-TPA-PE** (Table S2); primary natural transition orbitals (NTOs) and their coefficients (Figure S15); and excited-state potential energy surface and the corresponding properties, transition density maps for $S_0 \leftrightarrow S_1$ absorption/emission processes (Figure S16) (PDF)

Cif file for the single crystal of 2EHO-TPA-PE (CIF)

"Checkcif report" file for the single crystal of 2EHO-TPA-PE (PDF)

■ AUTHOR INFORMATION

Corresponding Authors

Hakan Usta − *Department of Nanotechnology Engineering, Abdullah Gül University, 38080 Kayseri, Turkey;* orcid.org/0000-0002-0618-1979; Email: hakan.usta@agu.edu.tr

Bunyemin Cosut − *Department of Chemistry, Gebze Technical University, 41400 Gebze, Kocaeli, Turkey;* orcid.org/0000-0001-6530-0205; Email: bc@gtu.edu.tr

Fahri Alkan − *Department of Nanotechnology Engineering, Abdullah Gül University, 38080 Kayseri, Turkey;* orcid.org/0000-0002-4046-9044; Email: fahri.alkan@agu.edu.tr

Complete contact information is available at: https://pubs.acs.org/10.1021/acs.jpcb.1c07165

Notes

The authors declare no competing financial interest.

Additional crystallographic data for 2EHO-TPA-PE with the CCDC reference number 2100811 has been deposited within the Cambridge Crystallographic Data Center via www.ccdc.cam.ac.uk/deposit

■ ACKNOWLEDGMENTS

H.U. acknowledges support from the Scientific and Technological Research Council of Turkey (TUBITAK), Grant No. 113G035. We thank Prof. Turan Ozturk and Dr. Dilek Alimli for their help with the quantum efficiency measurements using the integrating-sphere method.

■ REFERENCES

(1) Qiu, X.; Ying, S.; Wang, C.; Hanif, M.; Xu, Y.; Li, Y.; Zhao, R.; Hu, D.; Ma, D.; Ma, Y. Novel 9,9-Dimethylfluorene-Bridged D−π−A-Type Fluorophores with a Hybridized Local and Charge-Transfer Excited State for Deep-Blue Electroluminescence with CIE y ∼ 0.05. *J. Mater. Chem. C* **2019**, *7*, 592−600.

(2) Xu, Y.; Xu, P.; Hu, D.; Ma, Y. Recent Progress in Hot Exciton Materials for Organic Light-Emitting Diodes. *Chem. Soc. Rev.* **2021**, *50*, 1030−1069.

(3) Zhou, C.; Cong, D.; Gao, Y.; Liu, H.; Li, J.; Zhang, S.; Su, Q.; Wu, Q.; Yang, B. Enhancing the Electroluminescent Efficiency of Acridine-Based Donor−Acceptor Materials: Quasi-Equivalent Hybridized Local and Charge-Transfer State. *J. Phys. Chem. C* **2018**, *122*, 18376−18382.

(4) Zhang, W.; Kong, J.; Hu, D.; Tao, M.; Niu, X.; Vdović, S.; Aumiler, D.; Ma, Y.; Xia, A. Solvation-Dependent Excited-State Dynamics of Donor−Acceptor Molecules with Hybridized Local and Charge Transfer Character. *J. Phys. Chem. C* **2020**, *124*, 5574−5582.

(5) Ebata, H.; Izawa, T.; Miyazaki, E.; Takimiya, K.; Ikeda, M.; Kuwabara, H.; Yui, T. Highly Soluble [1]Benzothieno[3,2- b]Benzothiophene (BTBT) Derivatives for High-Performance, Solution-Processed Organic Field-Effect Transistors. *J. Am. Chem. Soc.* **2007**, *129*, 15732−15733.

(6) Pujar, P.; Gandla, S.; Gupta, D.; Kim, S.; Kim, M. Trends in Low-Temperature Combustion Derived Thin Films for Solution-Processed Electronics. *Adv. Electron. Mater.* **2020**, *6*, 2000464.

(7) Takimiya, K.; Osaka, I.; Mori, T.; Nakano, M. Organic Semiconductors Based on [1]Benzothieno[3,2- b][1]Benzothiophene Substructure. *Acc. Chem. Res.* **2014**, *47*, 1493−1502.

(8) Lin, Z.; Kabe, R.; Wang, K.; Adachi, C. Influence of Energy Gap between Charge-Transfer and Locally Excited States on Organic Long Persistence Luminescence. *Nat. Commun.* **2020**, *11*, 191.

(9) Xu, Y.; Liang, X.; Zhou, X.; Yuan, P.; Zhou, J.; Wang, C.; Li, B.; Hu, D.; Qiao, X.; Jiang, X.; et al. Highly Efficient Blue Fluorescent OLEDs Based on Upper Level Triplet−Singlet Intersystem Crossing. *Adv. Mater.* **2019**, *31*, 1807388.

(10) Kim, T.; Xu, M.; Lee, Y. J.; Ku, K. H.; Shin, D. J.; Lee, D. C.; Jang, S. G.; Yun, H.; Kim, B. J. Fluorescence Switchable Block Copolymer Particles with Doubly Alternate-Layered Nanoparticle Arrays. *Small* **2021**, *17*, 2101222.

(11) Chen, H.; Shi, M.; Liu, M.; Xing, X.; Zhao, C.; Miao, J.; Ali, M. U.; Facchetti, A.; Meng, H. Host-Free Deep-Blue Organic Light-Emitting Transistors Based on a Novel Fluorescent Emitter. *ACS Appl. Mater. Interfaces* **2020**, *12*, 40558−40565.

(12) Usta, H.; Sheets, W. C.; Denti, M.; Generali, G.; Capelli, R.; Lu, S.; Yu, X.; Muccini, M.; Facchetti, A. Perfluoroalkyl-Functionalized Thiazole−Thiophene Oligomers as N-Channel Semiconductors in Organic Field-Effect and Light-Emitting Transistors. *Chem. Mater.* **2014**, *26*, 6542−6556.

(13) Liu, Q.; Chavhan, S.; Zhang, H.; Sun, H.; Brock, A. J.; Manzhos, S.; Chen, Y.; Feron, K.; Bottle, S. E.; McMurtrie, J. C.; et al. Short Alkyl Chain Engineering Modulation on Naphthalene Flanked Diketopyrrolopyrrole toward High-Performance Single Crystal Transistors and Organic Thin Film Displays. *Adv. Electron. Mater.* **2021**, *7*, 2000804.

(14) Zhu, H.; Shin, E.; Liu, A.; Ji, D.; Xu, Y.; Noh, Y. Printable Semiconductors for Backplane TFTs of Flexible OLED Displays. *Adv. Funct. Mater.* **2020**, *30*, 1904588.

(15) Baeg, K.-J.; Binda, M.; Natali, D.; Caironi, M.; Noh, Y.-Y. Organic Light Detectors: Photodiodes and Phototransistors. *Adv. Mater.* **2013**, *25*, 4267−4295.

(16) Le, M. N.; Baeg, K.; Kim, K. K.; Kang, S.; Choi, B. D.; Park, C.; Jeon, S.; Lee, S.; Jo, J.; Kim, S.; et al. Versatile Solution-Processed Organic−Inorganic Hybrid Superlattices for Ultraflexible and Transparent High-Performance Optoelectronic Devices. *Adv. Funct. Mater.* **2021**, *31*, 2103285.

(17) Baldo, M. A.; O'Brien, D. F.; You, Y.; Shoustikov, A.; Sibley, S.; Thompson, M. E.; Forrest, S. R. Highly Efficient Phosphorescent Emission from Organic Electroluminescent Devices. *Nature* **1998**, *395*, 151−154.

(18) Liu, T.; Chen, X.; Zhao, J.; Wei, W.; Mao, Z.; Wu, W.; Jiao, S.; Liu, Y.; Yang, Z.; Chi, Z. Hybridized Local and Charge-Transfer Excited State Fluorophores Enabling Organic Light-Emitting Diodes with Record High Efficiencies Close to 20%. *Chem. Sci.* **2021**, *12*, 5171−5176.
(19) Li, D.; Yang, J.; Wang, Y.; Li, X.; Zhu, D.; Fang, M.; Li, Z. Bright Mechanoluminescent Luminogens Even in Daylight through Close Intermolecular Interaction with the Characteristic of Hybridized Local and Charge Transfer (HLCT). *J. Mater. Chem. C* **2020**, *8*, 10852−10858.
(20) Lv, C.; Liu, W.; Luo, Q.; Yi, H.; Yu, H.; Yang, Z.; Zou, B.; Zhang, Y. A Highly Emissive AIE-Active Luminophore Exhibiting Deep-Red to near-Infrared Piezochromism and High-Quality Lasing. *Chem. Sci.* **2020**, *11*, 4007−4015.
(21) Fan, J.; Cai, L.; Lin, L.; Wang, C. Dynamics of Excited States for Fluorescent Emitters with Hybridized Local and Charge-Transfer Excited State in Solid Phase: A QM/MM Study. *J. Phys. Chem. A* **2016**, *120*, 9422−9430.
(22) Li, W.; Liu, D.; Shen, F.; Ma, D.; Wang, Z.; Feng, T.; Xu, Y.; Yang, B.; Ma, Y. A Twisting Donor-Acceptor Molecule with an Intercrossed Excited State for Highly Efficient, Deep-Blue Electroluminescence. *Adv. Funct. Mater.* **2012**, *22*, 2797−2803.
(23) Turro, N. J. *Modern Molecular Photochemistry*; University Science Books: Sausalito, CA, 1991.
(24) Komino, T.; Nomura, H.; Koyanagi, T.; Adachi, C. Suppression of Efficiency Roll-Off Characteristics in Thermally Activated Delayed Fluorescence Based Organic Light-Emitting Diodes Using Randomly Oriented Host Molecules. *Chem. Mater.* **2013**, *25*, 3038−3047.
(25) Yu, Y.; Ma, L.; Feng, Z.; Liu, B.; Zhou, H.; Qin, H.; Li, H.; Song, J.; Zhou, G.; Wu, Z. Strategy for Achieving Efficient Electroluminescence with Reduced Efficiency Roll-off: Enhancement of Hot Excitons Spin Mixing and Restriction of Internal Conversion by Twisted Structure Regulation Using an Anthracene Derivative. *J. Mater. Chem. C* **2019**, *7*, 5604−5614.
(26) Segal, M.; Singh, M.; Rivoire, K.; Difley, S.; Van Voorhis, T.; Baldo, M. A. Extrafluorescent Electroluminescence in Organic Light-Emitting Devices. *Nat. Mater.* **2007**, *6*, 374−378.
(27) Li, W.; Pan, Y.; Yao, L.; Liu, H.; Zhang, S.; Wang, C.; Shen, F.; Lu, P.; Yang, B.; Ma, Y. A Hybridized Local and Charge-Transfer Excited State for Highly Efficient Fluorescent OLEDs: Molecular Design, Spectral Character, and Full Exciton Utilization. *Adv. Opt. Mater.* **2014**, *2*, 892−901.
(28) Yamaguchi, Y.; Ochi, T.; Miyamura, S.; Tanaka, T.; Kobayashi, S.; Wakamiya, T.; Matsubara, Y.; Yoshida, Z. Rigid Molecular Architectures That Comprise a 1,3,5-Trisubstituted Benzene Core and Three Oligoaryleneethynylene Arms: Light-Emitting Characteristics and π Conjugation between the Arms. *J. Am. Chem. Soc.* **2006**, *128*, 4504−4505.
(29) Yamaguchi, Y.; Matsubara, Y.; Ochi, T.; Wakamiya, T.; Yoshida, Z. How the π Conjugation Length Affects the Fluorescence Emission Efficiency. *J. Am. Chem. Soc.* **2008**, *130*, 13867−13869.
(30) Yamaguchi, Y.; Ochi, T.; Matsubara, Y.; Yoshida, Z. I. Highly Emissive Whole Rainbow Fluorophores Consisting of 1,4-Bis(2-Phenylethynyl)Benzene Core Skeleton: Design, Synthesis, and Light-Emitting Characteristics. *J. Phys. Chem. A* **2015**, *119*, 8630−8642.
(31) Ochi, T.; Yamaguchi, Y.; Wakamiya, T.; Matsubara, Y.; Yoshida, Z. I. Block Modification of Rod-Shaped π Conjugated Carbon Frameworks with Donor and Acceptor Groups toward Highly Fluorescent Molecules: Synthesis and Emission Characteristics. *Org. Biomol. Chem.* **2008**, *6*, 1222−1231.
(32) Ervithayasuporn, V.; Abe, J.; Wang, X.; Matsushima, T.; Murata, H.; Kawakami, Y. Synthesis, Characterization, and OLED Application of Oligo(p-Phenylene Ethynylene)s with Polyhedral Oligomeric Silsesquioxanes (POSS) as Pendant Groups. *Tetrahedron* **2010**, *66*, 9348−9355.
(33) Fenenko, L.; Shao, G.; Orita, A.; Yahiro, M.; Otera, J.; Svechnikov, S.; Adachi, C. Electrical Properties of 1,4-Bis(4-(Phenylethynyl)Phenylethynyl)Benzene and Its Application for Organic Light Emitting Diodes. *Chem. Commun.* **2007**, No. 22, 2278.
(34) Mao, G.; Orita, A.; Fenenko, L.; Yahiro, M.; Adachi, C.; Otera, J. Blue Emitting Fluorophores of Phenyleneethynylenes Substituted by Diphenylethenyl Terminal Groups for Organic Light-Emitting Diodes. *Mater. Chem. Phys.* **2009**, *115*, 378−384.
(35) Usta, H.; Alimli, D.; Ozdemir, R.; Dabak, S.; Zorlu, Y.; Alkan, F.; Tekin, E.; Can, A. Highly Efficient Deep-Blue Electroluminescence Based on a Solution-Processable A−π−D−π−A Oligo(p -Phenyleneethynylene) Small Molecule. *ACS Appl. Mater. Interfaces* **2019**, *11*, 44474−44486.
(36) Usta, H.; Alimli, D.; Ozdemir, R.; Tekin, E.; Alkan, F.; Kacar, R.; Altas, A. G.; Dabak, S.; Gürek, A. G.; Mutlugun, E.; et al. A Hybridized Local and Charge Transfer Excited State for Solution-Processed Non-Doped Green Electroluminescence Based on Oligo(p -Phenyleneethynylene). *J. Mater. Chem. C* **2020**, *8*, 8047−8060.
(37) Ozdemir, M.; Choi, D.; Zorlu, Y.; Cosut, B.; Kim, H.; Kim, C.; Usta, H. A New Rod-Shaped BODIPY-Acetylene Molecule for Solution-Processed Semiconducting Microribbons in n-Channel Organic Field-Effect Transistors. *New J. Chem.* **2017**, *41*, 6232−6240.
(38) Frisch, M. J.; Trucks, G. W.; Schlegel, H. B.; Scuseria, G. E.; Robb, M. A.; Cheeseman, J. R.; Scalmani, G.; Barone, V.; Mennucci, B.; Petersson, G. A.; et al. Gaussian 09. Gaussian Inc.: Wallingford, CT,2010.
(39) Lee, C.; Yang, W.; Parr, R. G. Development of the Colle-Salvetti Correlation-Energy Formula into a Functional of the Electron Density. *Phys. Rev. B: Condens. Matter Mater. Phys.* **1988**, *37*, 785−789.
(40) Becke, A. D. Density-functional Thermochemistry. III. The Role of Exact Exchange. *J. Chem. Phys.* **1993**, *98*, 5648−5652.
(41) Lu, T.; Chen, F. Multiwfn: A Multifunctional Wavefunction Analyzer. *J. Comput. Chem.* **2012**, *33*, 580−592.
(42) Peach, M. J. G.; Benfield, P.; Helgaker, T.; Tozer, D. J. Excitation Energies in Density Functional Theory: An Evaluation and a Diagnostic Test. *J. Chem. Phys.* **2008**, *128*, 044118.
(43) You, H.; Kang, H.; Kim, D.; Park, J. S.; Lee, J.; Lee, S.; Kim, F. S.; Kim, B. J. Cyano-Functionalized Quinoxaline-Based Polymer Acceptors for All-Polymer Solar Cells and Organic Transistors. *ChemSusChem* **2021**, *14*, 3520−3527.
(44) Usta, H.; Facchetti, A.; Marks, T. J. N -Channel Semiconductor Materials Design for Organic Complementary Circuits. *Acc. Chem. Res.* **2011**, *44*, 501−510.
(45) Jones, B. A.; Facchetti, A.; Marks, T. J.; Wasielewski, M. R. Cyanonaphthalene Diimide Semiconductors for Air-Stable, Flexible, and Optically Transparent n-Channel Field-Effect Transistors. *Chem. Mater.* **2007**, *19*, 2703−2705.
(46) Chinchilla, R.; Nájera, C. Recent Advances in Sonogashira Reactions. *Chem. Soc. Rev.* **2011**, *40*, 5084.
(47) Miyaura, N.; Suzuki, A. Palladium-Catalyzed Cross-Coupling Reactions of Organoboron Compounds. *Chem. Rev.* **1995**, *95*, 2457−2483.
(48) Costa, J. C. S.; Santos, L. M. N. B. F. Hole Transport Materials Based Thin Films: Topographic Structures and Phase Transition Thermodynamics of Triphenylamine Derivatives. *J. Phys. Chem. C* **2013**, *117*, 10919−10928.
(49) Tamoto, N.; Adachi, C.; Nagai, K. Electroluminescence of 1,3,4-Oxadiazole and Triphenylamine-Containing Molecules as an Emitter in Organic Multilayer Light Emitting Diodes. *Chem. Mater.* **1997**, *9*, 1077−1085.
(50) Li, Z. H.; Wong, M. S.; Fukutani, H.; Tao, Y. Full Emission Color Tuning in Bis-Dipolar Diphenylamino-Endcapped Oligoarylfluorenes. *Chem. Mater.* **2005**, *17*, 5032−5040.
(51) Gudeika, D.; Bundulis, A.; Mihailovs, I.; Volyniuk, D.; Rutkis, M.; Grazulevicius, J. V. Donor and Acceptor Substituted Triphenylamines Exhibiting Bipolar Charge-Transporting and NLO Properties. *Dyes Pigm.* **2017**, *140*, 431−440.
(52) Bondi, A. Van Der Waals Volumes and Radii. *J. Phys. Chem.* **1964**, *68*, 441−451.
(53) Cai, Y.; Samedov, K.; Albright, H.; Dolinar, B. S.; Guzei, I. A.; Hu, R.; Zhang, C.; Tang, B. Z.; West, R. High Solid-State Fluorescence in Ring-Shaped AEE-Active Tetraphenylsilole Derivatives. *Chem. Commun.* **2014**, *50*, 12714−12717.

https://doi.org/10.1021/acs.jpcb.1c07165
J. Phys. Chem. B 2021, 125, 11717−11731

(54) Kumar, N. S. S.; Varghese, S.; Rath, N. P.; Das, S. Solid State Optical Properties of 4-Alkoxy-Pyridine Butadiene Derivatives: Reversible Thermal Switching of Luminescence. *J. Phys. Chem. C* **2008**, *112*, 8429−8437.
(55) Dreuw, A.; Plötner, J.; Lorenz, L.; Wachtveitl, J.; Djanhan, J. E.; Brüning, J.; Metz, T.; Bolte, M.; Schmidt, M. U. Molecular Mechanism of the Solid-State Fluorescence Behavior of the Organic Pigment Yellow 101 and Its Derivatives. *Angew. Chem., Int. Ed.* **2005**, *44*, 7783−7786.
(56) Langhals, H.; Potrawa, T.; Noth, H.; Linti, G. The Influence of Packing Effects on the Solid-State Fluorescence of Diketopyrrolopyrroles. *Angew. Chem., Int. Ed. Engl.* **1989**, *28*, 478−480.
(57) Cai, Y.; Samedov, K.; Dolinar, B. S.; Albright, H.; Song, Z.; Zhang, C.; Tang, B. Z.; West, R. AEE-Active Cyclic Tetraphenylsilole Derivatives with ∼ 100% Solid-State Fluorescence Quantum Efficiency. *Dalt. Trans.* **2015**, *44*, 12970−12975.
(58) Fu, C.; Luo, S.; Li, Z.; Ai, X.; Pang, Z.; Li, C.; Chen, K.; Zhou, L.; Li, F.; Huang, Y.; et al. Highly Efficient Deep-Blue OLEDs Based on Hybridized Local and Charge-Transfer Emitters Bearing Pyrene as the Structural Unit. *Chem. Commun.* **2019**, *55*, 6317−6320.
(59) Yao, L.; Zhang, S.; Wang, R.; Li, W.; Shen, F.; Yang, B.; Ma, Y. Highly Efficient Near-Infrared Organic Light-Emitting Diode Based on a Butterfly-Shaped Donor-Acceptor Chromophore with Strong Solid-State Fluorescence and a Large Proportion of Radiative Excitons. *Angew. Chem., Int. Ed.* **2014**, *53*, 2119−2123.
(60) Jayabharathi, J.; Panimozhi, S.; Thanikachalam, V. Hot Exciton Transition for Organic Light-Emitting Diodes: Tailoring Excited-State Properties and Electroluminescence Performances of Donor−Spacer−Acceptor Molecules. *RSC Adv.* **2018**, *8*, 37324−37338.
(61) Gao, Y.; Zhang, S.; Pan, Y.; Yao, L.; Liu, H.; Guo, Y.; Gu, Q.; Yang, B.; Ma, Y. Hybridization and De-Hybridization between the Locally-Excited (LE) State and the Charge-Transfer (CT) State: A Combined Experimental and Theoretical Study. *Phys. Chem. Chem. Phys.* **2016**, *18*, 24176−24184.
(62) Dereka, B.; Rosspeintner, A.; Li, Z.; Liska, R.; Vauthey, E. Direct Visualization of Excited-State Symmetry Breaking Using Ultrafast Time-Resolved Infrared Spectroscopy. *J. Am. Chem. Soc.* **2016**, *138*, 4643−4649.
(63) Rout, Y.; Cesaretti, A.; Ferraguzzi, E.; Carlotti, B.; Misra, R. Multiple Intramolecular Charge Transfers in Multimodular Donor−Acceptor Chromophores with Large Two-Photon Absorption. *J. Phys. Chem. C* **2020**, *124*, 24631−24643.
(64) Niu, X.; Kuang, Z.; Planells, M.; Guo, Y.; Robertson, N.; Xia, A. Electron-Donating Strength Dependent Symmetry Breaking Charge Transfer Dynamics of Quadrupolar Molecules. *Phys. Chem. Chem. Phys.* **2020**, *22*, 15743−15750.
(65) Dereka, B.; Vauthey, E. Solute−Solvent Interactions and Excited-State Symmetry Breaking: Beyond the Dipole−Dipole and the Hydrogen-Bond Interactions. *J. Phys. Chem. Lett.* **2017**, *8* (16), 3927−3932.
(66) Liu, T.; Zhu, L.; Zhong, C.; Xie, G.; Gong, S.; Fang, J.; Ma, D.; Yang, C. Naphthothiadiazole-Based Near-Infrared Emitter with a Photoluminescence Quantum Yield of 60% in Neat Film and External Quantum Efficiencies of up to 3.9% in Nondoped OLEDs. *Adv. Funct. Mater.* **2017**, *27*, 1606384.
(67) Song, H.; Wang, K.; Kuang, Z.; Zhao, Y. S.; Guo, Q.; Xia, A. Solvent Modulated Excited State Processes of Push−Pull Molecule with Hybridized Local Excitation and Intramolecular Charge Transfer Character. *Phys. Chem. Chem. Phys.* **2019**, *21*, 3894−3902.
(68) Li, C.; Hanif, M.; Li, X.; Zhang, S.; Xie, Z.; Liu, L.; Yang, B.; Su, S.; Ma, Y. Effect of Cyano-Substitution in Distyrylbenzene Derivatives on Their Fluorescence and Electroluminescence Properties. *J. Mater. Chem. C* **2016**, *4*, 7478−7484.
(69) Xie, W.; Li, B.; Cai, X.; Li, M.; Qiao, Z.; Tang, X.; Liu, K.; Gu, C.; Ma, Y.; Su, S.-J. Thiophene Disubstituted Benzothiadiazole Derivatives: An Effective Planarization Strategy Toward Deep-Red to Near-Infrared (NIR) Organic Light-Emitting Diodes. *Front. Chem.* **2019**, *7*, 276.

https://doi.org/10.1021/acs.jpcb.1c07165
J. Phys. Chem. B 2021, 125, 11717−11731